X-524-66-246

NASA TM X-55539

A FOCUS SPOILING RETRODIRECTIVE MODULATOR

BY
MICHAEL W. FITZMAURICE

GPO PRICE $ _____

CFSTI PRICE(S) $ _____

MAY 1966

Hard copy (HC) 3.00

Microfiche (MF) .75

ff 653 July 65

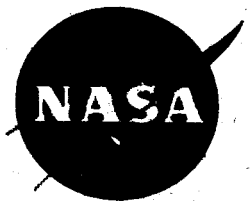

GODDARD SPACE FLIGHT CENTER
GREENBELT, MD.

A FOCUS SPOILING RETRODIRECTIVE MODULATOR

by

Michael W. Fitzmaurice

May 1966

APPROVED:

Henry H. Plotkin, Head
Optical Systems Branch

Robert J. Coates, Chief
Advanced Development Division

Goddard Space Flight Center
Greenbelt, Maryland

ABSTRACT

30362

The continually increasing need for greater information channel capacity between orbiting spacecraft and ground has stimulated much investigation into the possible applicability of lasers. This paper analyzes a semi-passive optical modulator which can be incorporated into a satellite to ground laser communication link or a ground to ground laser link. The system has limited bandwidth capabilities but is useful as a first step in evaluating the utility of lasers in communication through the earth's atmosphere.

Modulation is imposed on a reflected beam by varying the optical properties of the retrodirector by a piezoelectric induced displacement.

An analysis of the piezoelectric transducer is carried out and equations developed which are used in a typical design procedure. Particular emphasis is placed on the modulator power requirements as a function of bandwidth.

Experimentally, the validity of a geometrical optics approach to the modulation capabilities of the retrodirector is verified. In addition, the need for high speed displacement measurement techniques is noted and two solutions are presented. The first, employing an accelerometer, offers extreme accuracy but relatively narrow frequency response. The second approach utilizes the fringe pattern in a Michelson interferometer and has reduced accuracy but virtually unlimited frequency response.

ACKNOWLEDGMENTS

The author wishes to express his appreciation to Peter O. Minott (Goddard Space Flight Center) and Dr. U. Hochuli (University of Maryland) for their assistance and guidance during the development of this paper.

TABLE OF CONTENTS

GLOSSARY

a - wave velocity

a_i - mode constant

a_R - retrodirector aperture

a_T - receiver aperture

A - transducer cross-sectional area

A_R - retrodirector area

A_T - receiver area

c - damping coefficient

D - satellite range

D' - flexural rigidity

e - strain

E - energy parameter

E_y - Young's modulus

E_m - energy parameter

f - vibratory frequency

df - bandwidth

f_R - retrodirector secondary focal length

$f_{R'}$ - retrodirector primary focal length

f_T - equivalent receiver focal length

F_0 - peak driving force

g - gravitational constant

h - secondary mirror thickness

j - angular frequency

k - spring constant

K - coupling coefficient

m - mass of vibrating element

GLOSSARY (Continued)

n - Poisson's ratio

p - power dissipation

P_n - normalized power parameter

P_r - power received at ground station

P_T - power transmitted from ground station

q - atmospheric transmission

Q - quality factor

s - stress

t - secondary displacement

u - displacement variable

v - displacement variable

w - transducer weight per unit volume

W - secondary mirror weight

W_{cyc} - energy dissipated per vibratory cycle

x - object displacement from focal plane

x' - image location from focal plane

z - displacement of mass "m"

Z - peak value of displacement

α - phase angle between the driving force and the displacement

Δ - damping ratio

ω - circular frequency

ω_n - undamped natural frequency

$d\omega$ - 3 db bandwidth

λ - radiation wavelength

θ_R - retrodirector beam divergence

θ_T - transmitted beam divergence

LIST OF FIGURES

LIST OF FIGURES (Continued)

SECTION I

INTRODUCTION

The number of uses proposed for lasers in recent years has more than kept pace with their technological development. Nowhere has interest been keener than in the field of communications where the advent of a quasi-coherent oscillator at optical frequencies has presented the possibility of startling advances in bandwidth capabilities. Equally important is the fact that an optical carrier permits highly directional beams to be transmitted due to the inverse relationship of beam divergence and radiated frequency.* As a consequence of these most desirable virtues, coherence at an optical frequency, multifarious applications present themselves and, indeed, in some fields (e.g. medicine) have already proved uniquely successful. Complete fulfillment in the communications domain, however, must await the development of modulators and detectors with bandwidths far greater than the present state-of-the-art. Presently available traveling wave phototube detectors are limited to the low gigacycle range,** which is not significantly different from developed microwave technology. Electro-optical modulators have similar bandwidth capabilities and in general require considerable power. In addition, if one intends to take full advantage of the high directivity characteristic of laser radiation, he must be able to point his transmitter (in this case, an optical telescope) very accurately in order to insure target acquisition. This implies tracking accuracies on the order of a second of arc which is most difficult when one considers some of the problem areas such

*In the far field pattern, the half angle of beam divergence "θ" may be expressed as: $\theta \approx \lambda/a$, where "λ" is the wavelength of the radiation and "a" is a characteristic dimension of transmitter size.

**E.G. Sylvania Traveling Wave Microwave Phototube Type SY-4304

as atmospheric turbulence, mechanical deflections of the telescope, and shaft angle encoder limitations.

Nevertheless, much interest has been expressed in a laser communications link between an orbiting spacecraft and ground. For such a system, the aforementioned considerations on pointing accuracy immediately tend to negate the possibility of placing a laser transmitter in orbit. One system that has been proposed and which has several distinct advantages is shown in Figure 1. The key element in this system is a retrodirector which is aboard the spacecraft. This retrodirector functionally is a unique type of mirror which has the property that it reflects incident light back along a path which is collinear with the input beam. Therefore if an orbiting retrodirector intercepts energy from a ground-based laser transmitter, it will reflect the light back to the transmitter. If, in addition, the retrodirector has a capability for modulating the reflected beam, and if a detector (such as a phototube) is located near the transmitter, then in essence, this system can affect the transfer of information from spacecraft to ground. This approach to a laser link is attractive in several respects.

First, both the transmitter and receiver are ground based and therefore readily accessible to monitoring and repair. Secondly, only one high accuracy tracking mount is required since both transmitter and receiver are at the same location. Third, although the transmitted beam must have a divergence sufficient to insure spacecraft acquisition, the retrodirected beam can be collimated to the diffraction limit.* This maximizes the energy density of the return beam thereby enhancing the signal to noise ratio at the receiver. Fourth, the power requirements

*An additional factor that should be considered is the displacement of the return beam due to the relative velocity existing between the spacecraft and the earth's surface. If this effect, called velocity aberration, results in an appreciable displacement, then either the receiver must be moved in the appropriate direction, or the return beam must have enough divergence so that the receiver remains within the cone of the return energy. For more information on this effect, the reader is referred to GSFC report X-524-63-59.

aboard the spacecraft are minimal as will be shown later in this report. Fifth, accurate spacecraft stabilization is not required.

In addition, if the special case is considered where the spacecraft is in a synchronous orbit, then acquisition by the transmitter becomes much easier and may well enable both the transmitted and retrodirected beam to be collimated to the diffraction limit.

The spacecraft to ground link just considered may be expanded into a relay type ground to ground link with a small increase in satellite complexity. This approach is illustrated in Figure 2. The information to be transmitted is put on beam "B" using any of well understood techniques now available. The fact that considerable power may be required for external-to-cavity modulation schemes is of little consequence for this ground based transmitter. A receiver aboard the spacecraft will demodulate the beam utilizing envelope detection and will condition the signal so that it can drive the modulator within the retrodirector. The laser transmitter at "A" also illuminates the spacecraft with an unmodulated beam. A portion of this energy is intercepted by the retrodirector and sent back to the receiver at "A". However, the return beam is now modulated with the information from beam "B", so the output of the detector at "A" has the desired information. The obvious limitation of the system as shown is its restriction to unidirectional information flow. This may be overcome quite simply by the addition of a receiver at "B"*. The system now becomes a two-way ground to ground link which has operational capabilities over distances of intercontinental magnitude.**

*The addition of the receiver at "B" constrains the system only to the degree that the modulators at "A" and "B" must operate at different frequencies.

**A thorough analysis of this system has been carried out in GSFC Report X-524-66-177 by Peter O. Minott.

SECTION II

RETRODIRECTOR

As mentioned previously, it is the retrodirector which is the crucial element in this system. A cross section of this device in its most elemental form is shown in Figure 3. The two spherical reflecting surfaces have the same center of curvature with the secondary located at the focal surface of the primary. Two rays are traced through the system to illustrate off-axis as well as on-axis operation. It is seen, then, that the size of the secondary determines the maximum allowable off-axis angle. Over the accepted field of view, this concentric system operates without having an apparent optical axis and is therefore free from off-axis aberrations such as coma, astigmatism, and distortion. When one considers rays which are not paraxial, however, spherical aberration becomes significant and must be corrected. Complete correction requires the addition of two elements (Figure 4). The first, a concentric corrector, has two spherical surfaces with a center of curvature identical with the two reflectors. This corrector removes nearly all of the spherical aberration*; however, there remains some residual aberration which can be eliminated by the addition of the aspheric. It should be noted that the curvature of the aspheric is grossly exaggerated in Figure 4. In reality it is a very weak lens with slopes approximately 1/14 the value of a Schmidt system of equal aperture. The addition of the concentric and aspheric correctors to the retrodirector is most important for acceptable optical performance but is not germane to the modulator design, which is the prime

*For a quantitative analysis of the performance of a corrected concentric optical system, the reader is referred to "Achievements in Optics," A. Bouwers, Elsevier Press, Inc., Houston, Texas, 1950.

subject of this report. With this in mind, the author now proceeds considering the retrodirector as the two element system of Figure 3.

SECTION III

MODULATION TECHNIQUES

If a light beam is to be modulated, then the retrodirector must be capable of varying some property of the beam in an intelligible manner in accordance with the information to be transmitted. Among the properties which describe a laser beam are first its power (or intensity) and second its angular spread (divergence). Each of these properties will now be considered from the viewpoint of modulation possibilities.

Ideally, if the retrodirector secondary was a mirror whose reflectivity could be varied by an electrical signal, then an incident beam could be intensity modulated and subsequently retrodirected to a receiver where an envelope detector would perform the demodulation. Such a variable reflectivity mirror has been synthesized by placing a partially reflecting mirror and a total reflector together in the form of a modified Fabry-Perot interferometer. This is illustrated in Figure 5, which shows the input beam "1" partially reflected off the first surface along path "3". The remainder of the beam "2" continues on until it is totally reflected along path "4". The net intensity of the retrodirected beam is found by superimposing the wavefronts represented by rays "3" and "4". The spacing "d" between the reflecting surfaces determines the phase difference between "3" and "4" and thereby controls the intensity of the retrodirected beam. The spacing is varied by fixing the position of the partial reflector and mounting the other reflector on the face of a piezoelectric disc. This disc has electrodes on each face and is driven in a thickness mode by the application of a voltage. A change in "d" of $\lambda/4$ results in a path difference between "3" and "4" of $\lambda/2$ or 180°. This of course is sufficient to give 100% modulation. Using typical constants for a

lead zirconate - lead titanate ceramic operating near resonance, a quarter wave displacement requires less than a 10-volt driving signal. Such a retrodirective modulator has been built and is regarded as a qualified success.* This approach is very attractive from the standpoint of modulator power requirement (which is in the 100 milliwatt range). Unfortunately, the problems posed in fabricating two well matched interfering spherical surfaces are formidable and have not yet been completely solved. In addition, difficulty has been encountered in realizing the high displacement amplification factors which are theoretically possible when the transducer is in a resonant condition.

The second modulation scheme to be considered deals with the angular divergence of the retrodirected beam. Very little analysis is now available on this approach and it is therefore the prime purpose of this report to evaluate this technique with particular emphasis on modulator power requirements and modulation capabilities. The controlled divergence of the retrodirected beam will be affected by a technique known as "focus spoiling," to which end the remainder of this report is devoted.

*This interference modulator was fabricated by General Precision Labs under a GSFC contract. In addition, a detailed analysis of this type modulator was performed under GSFC contract NAS 5-3745.

SECTION IV

FOCUS SPOILING MODULATION

The concept of transmitting information by varying the divergence of the retrodirected beam is illustrated in Figure 6. The ground based telescope functions as both the transmitter and receiver in this case but the transmitted beam has been omitted from Figure 6 for clarity purposes. The strength of the signal received at the telescope is dependent on telescope aperture and the energy density of the retrodirected beam. It follows directly then that if the beam divergence is caused to increase during some time interval (Δt), then the energy density of the beam at the receiver will decrease and thereby cause a decrease in the signal generated by the detector. It now becomes obvious that if it is possible to vary the retrodirected beam divergence continuously, then the signal emanating from the detector will vary in similar fashion and the capability exists for transmitting an analog signal from spacecraft to ground.

The method devised to control the beam divergence is shown in Figure 7A. The two element retrodirector is drawn with the secondary in three positions. When the secondary is located in the focal plane of the primary (i.e. "1"), the retrodirected beam is highly collimated and, in fact, with proper correction can be expected to approach the diffraction limit. If the secondary is now moved to position "2", then the collimating ability of the retrodirector is seriously degraded and the retrodirected beam will diverge as shown. Similarly, although not depicted in Figure 7, if the secondary was displaced from the primary focal plane to the "3" position, then the return beam would converge to a distant image point and after passing through this point would diverge in a similar fashion.

In order to determine the relationship between retrodirected beam divergence "θ" and secondary mirror displacement "t" measured from the primary focal plane, some assumptions are helpful.

It is intuitively obvious that the input energy to the retrodirector which is imaged in the primary focal plane will have a very small spot size. This implies that only a very small portion of the spherical surface of the secondary is being used when at position "1" (Figure 7A). In addition, if it is now assumed that only minute excursions from position "1" will be required in order to develop appreciable modulation, then the small curvature of the portion of the secondary being used at any time becomes negligible and the spherical surface may be replaced by a plane mirror for analytical purposes. In Figure 7B a plane mirror representing the secondary is shown in the three appropriate positions. It can be seen from the symmetry involved that a displacement of "t" (i.e. to the "2" position) results in a real image being formed "2t" distant from the primary focal plane. From identical considerations, a displacement to "3" causes a virtual image to appear at "-2t". It is these images which serve as the objects for the retrodirector optics.

One may then conclude that when the secondary mirror is located at "1", the return beam appears to be due to a point source located at the primary focus and therefore its divergence will be zero (neglecting diffraction and spherical aberration effects). In addition, if the secondary is displaced by "t", then the apparent source of the retrodirected energy shifts by "2t". It is now useful to consider the system of Figure 8. A single lens of aperture "a_R" and primary and secondary focal lengths "f_R" and "f_R'" is shown with a point source located at "f_R". As before, this source is imaged at infinity and therefore implies $\theta_R = 0$. If the point source is now displaced a distance "2t", an image is formed at a distance $(f_R' + x')$. The relationship between object and image location is expressible in

the Newtonian form of lens formula (Ref. 1),

1. $$xx' = f_R f_R'$$

Recognizing that image and object spaces are both in the same medium,

$$f_R = f_R'$$

2. $$\therefore xx' = f_R^2$$

The displacement shown results in a beam spread given by:

$$\theta_R = 2 \tan^{-1} \frac{a_R/2}{x' + f_R}$$

For small displacements,

$$x' >> f_R$$

$$\tan \theta_R \approx \theta_R$$

$$\therefore \theta_R = \frac{a_R}{x'}$$

Solving for x' and substituting into 2.,

$$x \left(\frac{a_R}{\theta_R}\right) = f_R^2$$

$$\therefore (2t) \left(\frac{a_R}{\theta_R}\right) = f_R^2$$

3. $$\therefore \theta_R = \frac{(2t)\,(a_R)}{f_R^2}$$

This equation expresses the relationship between the divergence of the retrodirected beam and the secondary mirror displacement "t" with "a_R" and "f_R" referring to the retrodirector aperture and focal length respectively. Equation 3 is plotted in Figure 9 for a retrodirector with $a_R = 4.00$ inches and $f_R = 5.00$ inches.

It should be noted at this point that the result expressed by equation 3 has been based solely on a geometrical optics approach. A more accurate analysis of the effects of secondary mirror displacements could be formulated starting with the Huygens-Fresnel integral representation of the field in the focal region. Such an analysis is complex* and was not deemed necessary in this case. It is one of the major purposes of the experimental portion of this report to show that the geometrical approach will, in fact, give accurate results.

In order to understand the effect of return beam divergence on the system modulation capabilities, it is necessary to evaluate the overall transfer function of the transmitted and received energy. In Figure 10, the pertinent parameters are shown. From geometrical considerations, it can easily be shown that the power received at the ground (P_r) is given by:

$$4. \qquad P_R = \frac{16 P_T q^2 A_R A_T}{\pi^2 D^4 \theta_T^2 \theta_R^2}$$

where the parameters are defined as follows:

P_T - Laser power transmitted

P_r - Retrodirected power received at the ground station

q - Atmospheric transmission

A_R - Effective retrodirective area

*A. Bonin, "Electromagnetic Field in the Neighborhood of the Focus of a Coherent Beam," Physical Review, Vol. 138, No. 6B, June 1965.

A_T - Receiver area

D - Satellite Range

θ_T - Transmitted beam divergence

θ_R - Retrodirected beam divergence

Our interest lies with the effect of θ_R upon received power at the ground station. Therefore, for a particular retrodirector in a specified orbit, and with some known transmitter power we define a normalized parameter "P_n" where "P_n" is given by,

5. $$P_n = \frac{(P_r)}{\frac{16 P_T q^2 A_R A_T}{\pi^2 D^4 \theta_T^2}} = \frac{1}{\theta_R^2}$$

Selecting a minimum value of "θ_R", it is now possible to evaluate qualitatively the variation of received signal strength with "θ_R". In Figure 11, equation 5 is plotted with the minimum value of θ_R selected as the diffraction limit of a four inch circular aperture emitting radiation of wavelength 6328Å. The positive increments in "θ_R" are related to the position of the secondary mirror in the retrodirector through equation 3, so the abscissa of Figure 11 may just as validly be thought of as "t", the displacement of the secondary mirror from the primary focal plane. It follows then that the value t = 0 requires the secondary to be at the prime focus and the ground station to be receiving the maximum signal. If the secondary is biased to point A of Figure 11, then small signal excursions about this operating point are possible. In this case, 50% modulation will require secondary movements of approximately .5 microns (peak-to-peak). It is apparent due to the nonlinearity of the characteristic curves that high modulation values will cause considerable distortion.

Similar plots of equation 5 are shown in Figure 12 for various values of minimum "θ_R". It is clear that the retrodirected beam divergence must be kept very small if the modulation is to be accomplished efficiently (i.e. with a minimum of secondary movement).

SECTION V.

LUMPED PARAMETER POWER ANALYSIS

In any system which is to be placed aboard a spacecraft, power consumption must be rated as a most important parameter. The ground to ground communication link of Figure 2 requires spacecraft power to operate the receiver as well as the modulator unit within the retrodirector. However, the receiver power consumption is a fairly well known quantity since standard and well defined electronic techniques can be used in this part of the system. In addition, the satellite to ground link of Figure 1 has as its sole dissipating element the modulator unit. It is therefore apparent that an evaluation of modulator dissipation will completely specify the spacecraft power requirements.

The modulator unit will be approximated by the lumped parameter system of Figure 13A. In this schematic a mass "m" is being driven in forced vibration by "$F_0 \sin\omega t$" and is being restrained by a spring of value "k" and a damping mechanism "c". From a free body diagram analysis, it is seen that the equation of motion can be written as,

$$m\ddot{z} = -c\dot{z} - kz + F_0 \sin\omega t$$

$$\therefore m\ddot{z} + c\dot{z} + kz = F_0 \sin\omega t \tag{6.}$$

The solution to this second order differential equation is in general the sum of the complimentary and the particular solution. The complimentary solution may be neglected since it represents the transient response which will quickly vanish. Assume for the particular solution,

$$z = Z \sin(\omega t - \alpha)$$

Evaluating the first two time derivatives and substituting into equation 6 gives,

$$- m\omega^2 Z \sin(\omega t - \alpha) + c\omega Z \cos(\omega t - \alpha) + k Z \sin(\omega t - \alpha)$$

$$- F_0 \sin\omega t = 0$$

$$\therefore m\omega^2 Z \sin(\omega t - \alpha) - c\omega Z \sin(\omega t - \alpha + \pi/2) + k Z \sin(\omega t - \alpha)$$

$$+ F_0 \sin\omega t = 0$$

Using the phasor diagram of Figure 13B it is readily seen that

$$Z = \frac{F_0}{\left[\left(k - m\omega^2\right)^2 + (c\omega)^2\right]^{1/2}} \qquad \tan\alpha = \frac{c\omega}{k - m\omega^2}$$

For a mass "m" being driven by an oscillating force $F = F_0 \sin\omega t$, the energy dissipated per cycle is,

$$W_{cyc} = \int_{cyc} F\,dz = \int_{cyc} F \frac{dz}{dt}\,dt = \int_{cyc} F \dot{z}\,dt$$

Substituting into the above equation and evaluating over a full period "T",

$$W_{cyc} = \int_0^T F_0 \sin\omega t \left[\omega Z \cos(\omega t - \alpha)\right] dt$$

$$= \omega F_0 Z \sin\alpha \left(\frac{T}{2}\right) = F_0 Z \pi \sin\alpha \left(\frac{\text{work}}{\text{cycle}}\right)$$

From the phasor plot of Figure 13B,

$$F_0 \sin\alpha = c\omega Z$$

$$\therefore W_{cyc} = \pi c\omega Z^2$$

Therefore, the energy dissipated per unit time (i.e. power) is expressible as,

$$p = \pi c\omega Z^2 f = \pi c\omega Z^2 \left(\frac{\omega}{2\pi}\right) = \frac{c\omega^2 Z^2}{2}$$

In order to arrange this equation in more meaningful terminology, additional terms must now be introduced. The damped natural frequency of the system (ω_N) is given by,

$$\omega_n = \left(\frac{k}{m}\right)^{1/2}$$

Also, the damping ratio "Δ" and the quality factor "Q" are given as,

$$\Delta = \frac{c}{2m\omega_n}$$

$$Q = \frac{\omega_n}{d\omega}$$

The "Q" of a vibration system is directly analogous to the quality factor of an electrical tuned circuit and therefore the bandwidth "$d\omega$" refers to the points of an amplitude-frequency plot where the displacement has fallen off to .707 of its value at ω_N. It can readily be shown (Reference 2) that for

$$Q >> 1, \qquad \Delta = \frac{1}{2Q}$$

$$\therefore c = 2\Delta m\omega_n = \frac{m\omega_n}{Q}$$

7. $$\therefore p = \frac{m\omega_n \omega^2 Z}{2Q} = \frac{m\omega^2 Z^2 d\omega}{2}$$

Rearranging into more useful form,

$$8. \qquad p = 4\pi^3 m Z^2 f^2 df$$

A consistent set of units for this equation are listed below,

p - watts

m - kg

Z - meters

f - cps

df - cps

This result (equation 8) is most useful if properly interpreted. In effect, the equation states that for a given resonant device of mass "m" and bandwidth "df", one can evaluate the power requirement for a sinusoidal oscillation as soon as an operating frequency (f) and a peak amplitude (Z) are chosen. It can be shown from Eq. 5 that if a retrodirector capable of returning a beam of six arc seconds divergence is considered, a peak-to-peak displacement of the secondary mirror of 1.0 micron will suffice to give 50% modulation. The curves of Figure 14 are based on such a displacement and show clearly the heavy dependence of power dissipation on modulator bandwidth for various values of "mf^2". Similarly a retrodirector with a θ_R minimum of 12 arc seconds requires a peak-to-peak displacement of 2.0 microns for 50% modulation. A set of power-bandwidth curves for this unit has been generated in Figure 15.

SECTION VI.

DISTRIBUTED MASS PIEZOELECTRIC TRANSDUCER

The lumped parameter system of Figure 13A is of course extremely idealized and is useful primarily for the development of equation 8. The question remains then, what method should be used for displacing the secondary mirror within the retrodirector so that modulation of the return beam may be accomplished. There are numerous techniques which might be considered. Electromagnetic, electrostatic and magnetostrictive effects are but a few of the possible methods. However, when one notes the displacement magnitude required, the necessity for a highly efficient conversion of energy from electrical to mechanical, and the requirement for operational bandwidths with significant information capacity, then piezoelectric drive appears to offer the most promise.

A typical piezoelectric transducer is shown in Figure 16. The configuration chosen is tubular with the direction of poling parallel to the tube axis (i.e. the x-axis). The ends of the tube are covered with a conductive material so that the drive signal and the tube length changes will be related through the d_{33} constant of the particular material.* There are several reasons for choosing this configuration. First, it is highly desirable to maximize transducer displacement for a given input voltage. This implies operation in a d_{33} mode. Secondly, the coupling coefficient "k" which equals the square root of the energy conversion efficiency is also greatest in the "33" mode. Third, the power-bandwidth curves of Figures 14 and 15 show that relatively low frequency operation is desirable.

*For those unfamiliar with the constants used to describe piezoelectric material, reference is made to "Piezoelectric Technology, Data for Designers," a Clevite publication. Also, the IEEE Article "Standards on Piezoelectric Crystals," April 1958 is most comprehensive.

However, low resonant frequency implies large transducer lengths "L". Therefore, if a solid cylinder were used rather than a tube, transducer mass would increase drastically and, as will be seen later, this would increase transducer power requirements. A detailed analysis of this transducer configuration will now be undertaken with the ultimate aim being to develop equations and curves which can be used in a design procedure.

The validity of this analysis is dependent on the following assumptions:

1. The tube material is homogeneous, elastic and obeys Hooke's Law.
2. Tube cross-sections remain plane during vibration and the particles in the cross-sections have motion only in the axial (x) direction. This is valid for $L >> t$.

In addition, the following quantities will be used in the development and are now defined:

E_y - Young's modulus

e - strain

s - stress

A - Cross-sectional area of the tube

w - Transducer weight per unit volume

g - Gravitational Constant

u - Displacement of a tube cross-section at some x.

In general,

$$u = f(x, t) \qquad \text{where } t \text{ is the time variable}$$

At the m-n cross-section, remove a differential slice of thickness "dx" and consider the forces acting on it. Using D'Alembert's principle and noting that the

mass of the differential element is (w A dx/g), (Fig. 16B)

$$\frac{-w\,A\,dx}{g}\,\frac{\partial^2 u}{\partial t^2} = s_x A - \left(s_x + ds_x\right) A = -ds_x A$$

$$\therefore\ ds_x - \frac{w}{g}\,dx\,\frac{\partial^2 u}{\partial t^2} = 0$$

In general, since s is a function of both time and axial location,

$$ds_x = \frac{\partial s_x}{\partial x}\,dx + \frac{\partial s_x}{\partial t}\,dt$$

If we now consider some instant of time,

$$ds_x = \frac{\partial s_x}{\partial x}\,dx$$

but,

$$s_x = e\,E_y = \frac{\partial u}{\partial x}\,E_y$$

$$\therefore\ ds_x = \frac{\partial^2 u}{\partial t^2}\,dx\,E_y$$

or,

$$\frac{w}{g}\,\frac{\partial^2 u}{\partial t^2} = E_y\,\frac{\partial^2 u}{\partial x^2}$$

Now defining "a",

$$a^2 = \frac{E_y\,g}{w}$$

$$\therefore \frac{\partial^2 u}{\partial t^2} = a^2 \frac{\partial^2 u}{\partial x^2}$$

This is the one dimensional wave equation which can be solved by the method of separation of variables. Let "u" equal a product function of the type

$$u = X(x)\,T(t)$$

Substituting into the wave equation and dividing by XT,

$$\frac{\ddot{T}}{T} = a^2 \frac{X''}{X}$$

where the dots represent differentiation with respect to time and the primes denote differentiation with respect to position (x). In order for this equation to hold true when one of the variables is held constant and the other varied, the equation must be set equal to a constant. In a similar vein, in order to get a physically realizable solution, the constant must be of the form "$-j^2$" so that our resulting solutions are harmonic.

$$\therefore \frac{\ddot{T}}{T} = a^2 \frac{X''}{X} = -j^2$$

So the resulting solutions for T and X are:

$$T = A\cos jt + B\sin jt$$

$$X = C\cos(j/a)x + D\sin(j/a)x \qquad (9.)$$

The constants C and D can be evaluated from the boundary conditions while A and B are evaluated by use of the initial conditions. Now consider the case of

a long tube with both ends free. Then, the following boundary conditions exist,

1. At $x = 0$, $s = 0$ and $\therefore \frac{\partial u}{\partial x} = 0$

This implies $X'(0) = 0$

2. At $x = L$, $\frac{\partial u}{\partial x} = 0$

Similarly, this implies $X'(L) = 0$

From differentiation of equation 9,

$$X' = -C\, j/a \sin (j/a)\, x + D\, j/a \cos (j/a)\, x$$

From the first boundary condition, $D = 0$. Now applying the second boundary condition

$$0 = -C\, j/a \sin (j/a)\, L$$

This is the frequency equation for the system. For nontrivial solutions, $C \neq 0$ and therefore,

$$(j/a)\, L = i\pi \qquad i = 1, 2, \cdots$$

10. $$\therefore j_i = \frac{i\pi a}{L}$$

This relationship gives the natural frequencies for the tube. Considering the fundamental resonant condition, i.e. $i = 1$,

$$j_i = \frac{\pi a}{L} = 2\pi f_1$$

11. $$\therefore f_1 = \frac{a}{2L} = \frac{1}{2L}\left(\frac{E_y\, g}{w}\right)^{1/2}$$

In order to maximize the usefulness of the piezoelectric effect, it is necessary to consider the case where one end of the tube is fixed to a rigid base and the other end is free to expand. These boundary conditions are expressible as:

1. At $x = 0$ $\quad u(0, t) = 0$ (fixed end)

2. At $x = L$ $\quad \frac{\partial u(L, t)}{\partial x} = 0$ (free end)

Using the first boundary condition, $C = 0$. Similarly, from the second,

$$X' = D\, j/a \cos (j/a)\, x$$

$$\therefore 0 = D\, j/a \cos (j/a)\, L$$

So, neglecting the travial case where $D = 0$,

$$\cos (j/a)\, L = 0$$

$$\therefore j\, L/a = \frac{i\pi}{2} \qquad \text{where} \qquad i = 1, 3, 5, \cdots$$

$$\therefore j = \frac{i\pi a}{2L}$$

Considering the fundamental mode,

12. $$j_1 = \frac{\pi a}{2L}$$

So it is apparent that the effect of fixing one end of the tube was to reduce the lowest frequency to half its original value. The stiffness of a piezoelectric

element is dependent on the boundary conditions of its electrodes. This dependence is expressible quantitatively as: $E_{oc}^{(1-K^2)} = E_{sc}$

where E_{oc} - Modulus of elasticity (open circuited electrodes)

E_{sc} - Modulus of elasticity (short circuited electrodes)

K - Coupling coefficient (previously defined)

It follows from this that the material will be somewhat more compliant with its electrodes short-circuited. One may expect in an actual application that the driver amplifier for the modulating element will approximate a voltage source whose Thevenin equivalent impedance will be quite small. Therefore, E_{sc} will be used as the Modulus of Elasticity. For a lead titanate-lead zirconate composition such as pzt-4, (Ref. 4)

$$E_{sc} = \frac{1}{s_{33}^{E}} = \frac{1}{15.5 \times 10^{-12}} \square 6.45 \times 10^{10} \left(\frac{\text{Newton}}{\text{Meter}^2}\right)$$

$$\frac{w}{g} = 7.6 \times 10^{3} \left(\frac{\text{Kg}}{\text{Meter}^3}\right)$$

$$\therefore a = \left(\frac{Eg}{w}\right)^{1/2} = 2.92 \times 10^{3} \left(\frac{\text{Meter}}{\text{Sec}}\right)$$

From equation 12,

$$j_1 = \frac{\pi a}{2L} = 2\pi f_1$$

13. $$\therefore f_1 = \frac{a}{4L} = \frac{73.3 \times 10^{3}}{L}$$

where the tube length "L" is measured in cm., and the fundamental resonant frequency is in cps. This equation is plotted in Figure 17 and will prove to be of considerable utility in the final design of the modulator.

SECTION VII.

EFFECTS OF SECONDARY MIRROR ON TRANSDUCER CHARACTERISTICS

In order to more closely approach the physical situation in the modulator, the situation is now considered where there exists a tube with one end fixed and the other end attached to an object of weight W (Figure 16C). This weight will serve to illustrate the dynamic effect of the secondary mirror on the transducer just considered. An additional assumption must now be made. The stiffness of "W" is assumed to be much greater than that of the tube, and therefore the shift in resonant frequencies of the configuration will be dependent only on the added weight "W". This is a valid assumption if "L" is appreciably greater than "L′". The original development for a differential element utilizing D'Alembert's principle is unchanged and results again in the solution

$$u = XT$$

where

$$T = A \cos jt + B \sin jt$$

$$X = C \cos (j/a)x + D \sin (j/a)x$$

The following boundary conditions now appear:

$$\text{At } x = 0, \qquad u(0, t) = 0$$

and therefore $C = 0$ as before. At $x = L$, a free body diagram requires that the inertia and restoring forces be equal.

$$\therefore \frac{W}{g}\left(\frac{\partial^2 u}{\partial t^2}\right)_{x=L} = -s_{x=L} A$$

Also

$$s = e E_y = \frac{\partial u}{\partial x} E_y$$

$$\therefore \frac{W}{g}\left(\frac{\partial^2 u}{\partial t^2}\right)_{x=L} = -AE_y \left(\frac{\partial u}{\partial x}\right)_{x=L}$$

Substituting the second boundary condition from above gives:

$$\frac{W}{g}\left(-j^2 TX\right)_{x=L} = -AE_y \left(j/a\, D \cos (j/a) L\right) T$$

$$\therefore \frac{W}{g}\, j \sin (j/a) L = \frac{AE_y}{a} \cos (j/a) L$$

let

$$b = \frac{ALw}{W} \quad \text{and} \quad c = \frac{jL}{a}$$

(Note that "b" is actually the ratio of tube weight to the weight of "W"). Now the above equation can be rearranged into the form

$$c \tan c = b$$

This is the frequency equation for the system and can be solved graphically if a value of "b" is selected. Once again it is the lowest root of this equation which is of most interest since it corresponds to the fundamental resonant

frequency. Solutions for "c" are listed for various values of "b" (Reference 5):

b	.01	.10	.30	.50	.90	1.5	3.0	5.0	20	∞
c_1	.10	.32	.52	.65	.82	.98	1.20	1.32	1.52	$\pi/2$

Notice that if "W" gets very small, then "b" approaches infinity and,

$$c_1 = \pi/2$$

$$\therefore j_1 = \frac{a}{L} c_1 = \frac{a}{L} \frac{\pi}{2}$$

This of course is the same result as previously found for a tube without any "W" but with one end fixed. The result of the preceding development is plotted in Figure 18. The normalized frequency parameter (f/f_n) is the ratio of the fundamental resonant frequency of a tube with some "W" attached compared to the value prior to the addition of "W". Typically then, if the secondary mirror within the retrodirector weighs as much as the piezoelectric transducer, then the resonant frequency for the combination is approximately 55% of the unloaded value.

SECTION VIII.

TRANSDUCER EFFECTIVE MASS

In order to utilize the power relationship previously developed (equation 8) it is necessary to evaluate "m". It is clear that this quantity will be the sum of the secondary mirror mass and a portion of the distributed mass transducer.

Initially, considering the case where "W" is removed (i.e. b = ∞),

$$j_1 = \frac{a}{L} c_1 = \frac{a}{L} \frac{\pi}{2}$$

This first resonant frequency will now be redefined as "ω_n". For a lumped parameter system,

$$\omega_n = \left(\frac{k}{m}\right)^{1/2}$$

The spring constant of a long tube can be written as,

$$k = \frac{AE_y}{L}$$

So, setting our evaluated frequency ($a\pi/2L$) equal to a lumped parameter equivalent $(k/m)^{1/2}$, we can solve for a mass "m" which is really the effective dynamic mass (m_{eff}).

$$\therefore \frac{a}{L} \frac{\pi}{2} = \left(\frac{AE_y}{Lm_{eff.}}\right)^{1/2}$$

$$\therefore \frac{a^2 \pi^2}{4L^2} = \frac{AE_y}{Lm_{eff.}}$$

Putting in the previously defined value for "a^2" and simplifying gives:

$$m_{eff.} = 4/\pi^2 = .407 \text{ (Tube Mass)}$$

So it is apparent that dynamically, only 40.7% of the tube mass is acting. Now, if a weight "W" is added to the tube,

$$\left(\frac{k}{m_{eff.}}\right)^{1/2} = \frac{a}{L} c_1 = \frac{c_1}{L}\left(\frac{E_y g}{w}\right)^{1/2}$$

$$\therefore \frac{AE}{Lm_{eff.}} = \frac{c_1^2}{L^2}\frac{E_y g}{w}$$

or

$$m_{eff.} = \frac{ALw}{gc_1^2}$$

However, in this case, the effective mass (m_{eff}) is the sum of (W/g) plus a portion of the tube mass.

$$\therefore m_{eff.} = \frac{W}{g} + m_1 = \frac{ALw}{gc_1^2}$$

where "m_1" is the tube mass which is acting dynamically.

$$\therefore m_1 = \frac{ALw}{gc_1^2} - \frac{W}{g}$$

Since

$$b = \frac{\text{tube weight}}{W}$$

then

$$W = \frac{ALw}{b}$$

$$\therefore m_1 = \frac{ALw}{gc_1^2} - \frac{ALw}{gb} = (\text{Tube Mass})\left(\frac{1}{c_1^2} - \frac{1}{b}\right)$$

It becomes apparent that the percentage of the tube mass which is acting dynamically is a function of the weight ratio "b". However, when various sets of values for "b" and "c_1" are substituted into the above equation, it is found that the quantity $(1/c_1^2 - 1/b)$ is nearly constant and varies only between .35 - .40. So for power calculations, a value of .38 can be chosen for all "b" with negligible error.

SECTION IX.

SECONDARY MIRROR RIGIDITY CONSIDERATIONS

If the transducer driving the modulating mirror does not provide full support along the interface, as is the case in Figure 16C, then it becomes necessary to inspect the vibrational characteristics of the secondary. It is imperative for acceptable off-axis retrodirector performance that the moving mirror retain its spherical shape with the proper curvature. In addition, large deflections will induce tensile stresses which may easily exceed the strength of the glass. For ease of analysis we may approximate the secondary mirror by a flat circular plate of glass whose cross-section is as shown in Figure 19A. If the mirror is supported on one face at $r = r_0$ (Figure 19B), then the relationship for the normal mode frequencies is readily derived (Reference 5) and is of the form,

14. $$f_i = \frac{a_i}{2\pi r_0^2} \left(\frac{gD'}{wh}\right)^{1/2}$$

where

a_i - A constant depending on the mode of vibration being considered.

D' - The flexural rigidity defined as $Eh^3/12(1-n^2)$

n - Poisson's ratio

The other parameters in the equation remain as previously defined. The lowest value of "a_i" corresponds to the fundamental vibratory mode. In this case $a_i = 10.2$. Rearranging equation 14 and substituting in the following typical values

$E_y = 10 \times 10^6$ psi

$w = .1$ Lb/in^3

$n = .244$

$r_0 = 1.75/2$ inches

15. $\therefore f_1 = 124 \times 10^3 h$

where

h - inches

f_1 - cps

(It should be noted that the secondary mirror diameter chosen above corresponds to the retrodirector which was used in the experimental part of this report.)

If we apply to our design procedure the condition that the modulating frequency be a minimum of one octave below the fundamental resonance of the mirror, and selecting a typical modulating frequency as 50 kc, the preceding equations immediately lead to unacceptable performance characteristics.

i.e. $$h = \frac{100 \times 10^3}{124 \times 10^3} = .807 \text{ inches (Mirror Thickness)}$$

So the mirror weight is:

$$\frac{\pi}{4} (1.75)^2 (.807) (.1) (.454) = .088 \text{ Kg}$$

Neglecting momentarily the effective mass of the piezoelectric driver,

$$mf^2 = (.088) \left(5 \times 10^4\right)^2 = 2.2 \times 10^8 \text{ Kg/sec}^2$$

Referring to the graphs of Figures 14 and 15, it becomes obvious that the above value of mf^2 requires operation in a highly unfavorable portion of the power-bandwidth plots.

If the weight of the mirror is to be reduced, only the thickness dimension "h" can be varied since the diameter "r_0" is fixed by the field of view requirements of the optical system. So, in essence, there is a need to reduce the compliance of the mirror-transducer mount so that a thinner mirror can be used and still have operation one octave below resonance.

Perhaps the most obvious method of stiffening the assembly is to reduce the diameter of the piezoelectric tube and support the mirror at some radius "a" as shown in Figure 19C. This reduction in tube size offers the additional advantage of lowering the effective mass of the transducer. A confident design of the mirror-transducer assembly of Figure 19C requires a solution for the first normal mode frequency as a function of the support point "a". This writer, after a considerable search of the literature, concludes that a solution to this problem is not available and will, therefore, present an approximate solution based on the energy method of Lord Rayleigh (Reference 6).

The potential energy "U" of a plate undergoing a periodic displacement "v" can be shown to be expressible in polar coordinates as (Reference 5),

$$15.\quad U = \frac{D'}{2}\int_0^{2\pi}\int_0^{r_0}\left\{\left(\frac{\partial^2 v}{\partial r^2}+\frac{1}{r}\frac{\partial v}{\partial r}+\frac{1}{r^2}\frac{\partial^2 v}{\partial \theta_2}\right)^2 - 2(1-n)\frac{\partial^2 v}{\partial r^2}\left(\frac{1}{r}\frac{\partial v}{\partial r}+\frac{1}{r^2}\frac{\partial^2 v}{\partial \theta^2}\right) + 2(1-n)\left[\frac{\partial}{\partial r}\left(\frac{1}{r}\frac{\partial v}{\partial \theta}\right)\right]^2\right\} r\,dr\,d\theta$$

Our concern is the lowest mode which is symmetrical about the center. Therefore "U" will not vary with "θ" and 15 reduces to,

$$16.\quad U = \pi D'\int_0^{r_0}\left\{\left(\frac{d^2 v}{dr^2}+\frac{1}{r}\frac{dv}{dr}\right)^2 - 2(1-n)\frac{d^2 v}{dr^2}\frac{1}{r}\frac{dv}{dr}\right\} r\,dr$$

Similarly the kinetic energy "T" is given by,

$$T = \frac{wh}{2g} \int_0^{2\pi} \int_0^{r_0} \dot{v}^2 \, r \, dr \, d\theta$$

And if "θ" symmetry is present

17. $$T = \frac{\pi wh}{2g} \int_0^{r_0} \dot{v}^2 \, r \, dr$$

If we neglect the effects of damping, the transfer of energy from kinetic to potential is complete and for a conservative system such as this the maximum kinetic and potential energies can be equated. In general, "v" is a function of both time and position. However, in a normal mode, the time function is harmonic.

$$\therefore v = V_0 \cos jt$$

where V_0 is dependent only on "r" and will be selected in the form,

$$V_0 = a_1 \left(1 - \frac{r^2}{a^2}\right)^2 \text{, } a_1 \text{ being an arbitrary constant}$$

The choice of "V_0" is restricted only by the satisfying of the boundary conditions. Note, therefore, that both "V" and its first derivative vanish at r = a.

$$U_{max} = T_{max}$$

$$\therefore \pi D' \int_0^{r_0} \left\{ \left(\frac{d^2 V_0}{dr^2} + \frac{1}{r} \frac{dV_0}{dr} \right) - 2(1-n) \frac{d^2 V_0}{dr^2} \frac{1}{r} \frac{dV_0}{dr} \right\} r \, dr$$

$$= \frac{\pi wh}{g} \int_0^{r_0} V_0^2 \, j^2 \, r \, dr$$

Rearranging:

$$18.\int_0^{r_0}\left\{\frac{d^2V_0}{dr^2}+\frac{1}{r}\frac{dV_0}{dr}-2(1-n)\frac{d^2V_0}{dr^2}\frac{1}{r}\frac{dV_0}{dr}-\frac{whj^2V_0^2}{gD'}\right\}r\,dr \;=\; 0$$

Evaluating

$$\frac{dV_0}{dr}\,,\qquad \frac{d^2V_0}{dr^2}$$

and substituting into equation 18 gives,

$$\int_0^{r_0}\left\{\frac{64a_1^2}{a^4}-\frac{256a_1^2r^2}{a^6}+\frac{256a_1^2r^4}{a^8}-\frac{2a_1^2}{r}(1-n)\left(48\frac{r^5}{a^8}\right.\right.$$

$$\left.\left.-64\frac{r^3}{a^6}+16\frac{r}{a^4}\right)-\frac{whj^2V_0^2}{gD'}\right\}r\,dr \;=\; 0$$

Integrating, evaluating between the limits and simplifying gives,

$$\frac{64r_0^2}{a^4}-\frac{128r_0^4}{a^6}+\frac{256r_0^6}{3a^8}-4(1-n)\left\{\frac{8r_0^6}{a^8}-\frac{16r_0^4}{a^6}+\frac{8r_0^2}{a^4}\right\}$$

$$-\frac{2whj^2}{gD'}\left\{\frac{r_0^2}{2}-\frac{r_0^4}{a^2}+\frac{r_0^6}{a^4}-\frac{r_0^8}{2a^6}+\frac{r_0^{10}}{10a^8}\right\} \;=\; 0$$

Assigning a value of .244 to "n" and simplifying gives,

$$j^2 \;=\; \frac{gD'}{wh}\;\frac{\left[\frac{44.1}{a^4}-\frac{39.8r_0^2}{a^6}+\frac{30.5r_0^4}{a^8}\right]}{\left[.5-\frac{r_0^2}{a^2}+\frac{r_0^4}{a^4}-\frac{r_0^6}{2a^6}+\frac{r_0^8}{10a^8}\right]}$$

Note that j″ is the angular frequency in the harmonic time variation, so

$$j = 2\pi f$$

Also,

$$D' = \frac{E_y h^3}{12\left(1 - n^2\right)}$$

$$\therefore f = \frac{h}{2\pi}\left[\frac{gE_y\left(\frac{44.1}{a^4} - \frac{39.8\, r_0^2}{a^6} + \frac{30.5\, r_0^4}{a^8}\right)}{10.9\, w\left(.5 - \frac{r_0^2}{a^2} + \frac{r_0^4}{a^4} - \frac{r_0^6}{2a^6} + \frac{r_0^8}{10a^8}\right)}\right]^{1/2}$$

Let $y = r_0/a$

$$19. \qquad \therefore f = \frac{h}{2\pi r_0^2}\left[\frac{gE_y\left(44.1y^4 - 39.8y^6 + 30.5y^8\right)}{10.9\, w\left(.5 - y^2 + y^4 - y^6/2 + y^8/10\right)}\right]^{1/2}$$

This result is presented for the fundamental resonance of the circular plate supported circumferentially at "a" recognizing that the solution is approximate but useful in the absence of other analysis. It is interesting to note that neither of the eighth order polynomials under the radical of equation 19 has any real positive roots greater than unity. The existence of such a root would imply either zero or infinite compliance, both of which conditions are physically unacceptable in this case. In order to develop a feel for the effect of varying the tube diameter, let the mirror be supported at $.5\, r_0$.

$\therefore y = 2$ and substituting into equation 19, the ratio of the polynomials within the brackets is 1070. Expressing this result in terms of equation 14,

$$f_1 = \frac{32.7}{2\pi r_0^2}\left(\frac{gD'}{wh}\right)^{1/2}$$

and the net effect has been to increase the value of the first normal mode frequency by the factor (32.7/10.2). Once again the result is intuitively satisfying since in terms of equation 14, the change in support point has reduced "r_0" by a factor of 2, which change would tend to increase "a_i" by a factor of 4.

SECTION X.

TYPICAL MIRROR-TRANSDUCER DESIGN

Sufficient tools have been developed in the preceding sections so that it is now possible to proceed systematically with a typical modulator design. From a knowledge of the optical capabilities of the retrodirector, one can evaluate the magnitude of the peak secondary excursion required. A value of .5 microns will be selected in this example. (For a minimum retrodirected beam divergence of six arc seconds, this corresponds to 50 per cent modulation.) In addition, a center frequency of 30 kc will be chosen as a design goal. If the secondary mirror of diameter 1.75 inches is supported at $.5r_0$, then using equation 14 and the modifications of section IX,

$$h = \frac{60 \times 10^3}{3.2(124)\,10^3} = .151 \text{ inches}$$

Therefore, the secondary mass can be evaluated as,

$$m_{mirror} = \frac{\pi}{4}(1.75)^2(.151)(.1)(.454) = .0164\,Kg = 16.4\,gr$$

Selecting L = 1.0 cm, t = .15 cm

$$f_n = 73\,kc \text{ (Figure 17)}$$

$$m_{tube} = 2\pi Lwt\,(.5\,r_0) = 7.88 \text{ gr.}$$

$$\therefore m_{total} = m_{mirror} + m_{eff.\ tube}$$

$$= 16.4 + (.38)(7.88) = 19.4\,gr.$$

$$\therefore b = \frac{\text{tube weight}}{\text{mirror weight}} = \frac{7.88}{16.4} = .48$$

From Figure 18,

$$f/f_n = 41\%$$

$$\therefore f = .41\,(73\,kc) = 29.9\,kc$$

The modulator is shown full scale in Fig. 20 along with the power-bandwidth curve. In general, the design procedure outlined above is a trial and error method and will require judicious choices for "L" and "t".

It should be pointed out that all calculations up to this point have assumed a glass mirror. In general, the normal mode frequencies are proportional to $\left[E_y/w\right]^{1/2}$ (Eq. 14). For glass,

$$E_y/w \approx 100 \times 10^6$$

If beryllium was to be used,

$$E_{y/w} \approx 618 \times 10^6$$

So it is seen that beryllium will raise the resonant frequency by a factor of 2.48. This would normally imply that the mirror thickness could be drastically reduced. In reality, fabrication of high quality optical surfaces requires diameter-thickness ratios not appreciably greater than 10, and therefore the .15 cm thickness previously calculated cannot be seriously reduced.

Alternatively then, the effect of using beryllium would be to produce a very conservative design.

It is also possible that the secondary may be reduced in weight by using a rib-type structure at the transducer-mirror interface rather than a totally flat

surface. Properly designed, this would allow the mirror to maintain its dynamic rigidity while permitting some material to be cut off the back face.

As a concluding note to this section of the report it should be emphasized that an evaluation of the power requirements for a particular retrodirector will be heavily dependent upon the optical characteristics of the unit. The results expressed in fig. 20 are applicable only for the special case of a retrodirector with parameters (e.g., aperture, focal length, minimum beam divergence) which are identical with the assumed design values. These assumed values were selected from a unit which has been fabricated and which will be used in the experimental section of this report.

It is therefore expected that fig. 20 will be interpreted as order-of-magnitude results with the tacit understanding that a more accurate evaluation for a particular system is readily available using the equations and curves developed in this report.

SECTION XI.

EXPERIMENTAL VERIFICATION OF GEOMETRICAL ANALYSIS

The evaluation of the retrodirector undertaken in Section IV of this report and the result expressed by Equation 3 was based on the assumption that a geometrical optics analysis was sufficient. However, the electromagnetic field in a focal region is very complex, with wavefronts which are neither spherical nor plane (Reference 7, pg. 444). Consequently, there is a finite depth associated with the focused energy. Typically, for a f/1.25 system [using radiation of wavelength 6328A°], the depth of focus is approximately 2 microns. Recalling that the geometrical results of Section IV implied secondary mirror displacements of similiar magnitude, it becomes apparent that for a particular system, the modulating secondary mirror may remain within the region of the depth of focus during the entire oscillatory excursion. If this is the case, serious doubts may be raised about the validity of a ray trace analysis.

With this perspective, it was judged necessary to put together a laboratory system whose performance could be analyzed geometrically and evaluated experimentally. The subsequent comparison of the two sets of results would indicate the degree of accuracy obtainable with a geometrical optics approach.

The system layout is shown in Fig. 21. The CW laser output beam is increased to a diameter "a_T", collimated and transmitted to the retrodirector. The return beam is collinear and the portion which is transmitted by the beam splitter is imaged in the focal plane of the objective. The microscope objective B. forms a real magnified image of this spot at the appropriate conjugate point. The energy which passes through the field stop impinges on the cathode of the photomultiplier and results in a signal which is monitored on the oscilloscope.

It is convenient to consider this system in two distinct parts, a transmitter and a receiver.

The transmitter, consisting of the laser, microscope objective A. and the collimator objective merely furnishes a full aperture collimated beam to the retrodirector. The return beam is collected by the aperture "a_T" and the final image is formed at the field stop. Due to diffraction, this image will take the form of an Airy disc. Considerations of the size of this disc show that the receiving system (i.e., collimator objective and microscope objective B.) is equivalent to a system of aperture "a_T" and focal length "mf_0" where "m" is the power of the microscope objective and "f_0" is the focal length of the collimator objective.

In fig. 22, an equivalent receiver of focal length "$f_T = mf_0$" is shown with a field stop of diameter "D" located in the focal plane. This system will now be analyzed with the ultimate aim being to develop the relationship between the energy getting through the field stop and the input beam divergence "θ".

With input beam 1., an image will be formed in the focal plane. The field stop diameter "D" is selected so as to pass only the central bright portion of the Airy disc. The energy associated with this central portion will be designated "E_m". Now if the input beam has a total divergency "θ", then the image will be formed "x'" displaced from the focal plane and ergo the total energy "E" getting through the field stop will be reduced.

Using the Newtonian lens formula and proceding as in Section IV, it can be shown that the energy passing through the field stop is expressible as a function of "θ" in the following form:

20. $$E = \frac{E_m D^2}{a_T^2}\left(1 + \frac{2\,a_T}{f_T\,\theta} + \frac{a_T^2}{f_T^2\,\theta_T^2}\right)$$

The required field stop diameter "D" is, (reference 8)

21. $$D = 2.44\lambda \frac{f_T}{a_T}$$

where λ is the wavelength of the radiation being considered.

Substituting this into equation 20. and normalizing gives:

22. $$\frac{E}{E_m} = \frac{5.93\lambda^2 f_T^2}{a_T^4}\left(1 + \frac{2a_T}{f_T\theta} + \frac{a_T^2}{f_T^2\theta^2}\right)$$

The input beam to the receiver emanates from the retrodirector and therefore its divergence "θ" and the position of the secondary mirror within the retrodirector are related by equation 3.

23. $$\therefore \frac{E}{E_m} = \frac{5.93\lambda^2 f_T^2}{a_T^4}\left(1 + \frac{2a_T f_R^2}{f_T a_R t} + \frac{a_T^2 f_R^4}{a_R^2 f_T^2 t^2}\right)$$

This equation is plotted in Fig. 23 for the following laboratory parameters.

λ--------.6328 microns

f_T------100 meters

a_T------4.0 inches = .1 meters

f_R------5.0 inches = .125 meters

a_R------4.0 inches = .1 meters

This result which was obtained from a ray trace analysis can easily be checked experimentally if a square law detector (e.g., photomultiplier) is placed behind the field stop. The laboratory procedure is now outlined.

First an optical flat is used in place of the retrodirector so that lens B. may be accurately positioned to form an image at the field stop. Now removing the flat and using the retrodirector, the position of the secondary mirror is

adjusted until an image again appears at the field stop. This insures the proper secondary location. Using a field stop of appropriate size (Equation 21), the signal generated by the phototube is monitored on the oscilloscope. This reading will correspond to "E_m" of Equation 23. Adjusting the secondary position by means of the micrometer, it is now possible to give incremental displacements to the secondary mirror. The amount of energy reaching the detector will diminish accordingly and empirical curves can be traced and compared with the theoretical result of Equation 23.

This has been carried out in Figs. 24 and 25. In each case the theoretical curve decays at a somewhat larger rate that the empirical curve. However, the theoretical curve was based on the assumption that the energy density of the Airy disc was constant out to the first dark ring. More accurately, the intensity is described by a function of the form,

$$I \approx \left(\frac{2 J_1 (x)}{x}\right)^2$$

where J_1 is a Bessel function of the first kind

and x is the radius of the ring being considered.

An evaluation of this function shows that the intensity is down 3db at less than one-half the radius of the first minimum. This non-uniform intensity will tend to reduce the fall-off rate of the theoretical curves of Figs. 24 and 25.

Taking into consideration this inaccuracy in the theoretical development, it can be concluded that the laboratory data is in agreement with geometrical theory within the limits of experimental error.

SECTION XII

PIEZOELECTRIC DISPLACEMENT MEASUREMENTS

Proper operation of a focus spoiling modulator is critically dependent on the realization of relatively high secondary mirror displacements. The "d" constants for lead titanate-lead zirconate ceramics which are quoted in the literature are applicable to static conditions only and therefore may not accurately predict transducer response at a particular frequency. In addition, it is well known that the high "Q" values specified by the manufacturers suffer serious degradation at high stress levels.* Therefore, the need for a system which can measure the dynamic response of piezoelectric transducers is apparent.

One approach to this problem is illustrated in Fig. 26. An accelerometer (Endevco Model 2226) was mounted on the free face of a piezoelectric disc which is driven in a thickness mode by a variable frequency voltage "V_{in}". The accelerometer generated a voltage proportional to acceleration. However, for harmonic motion, acceleration and displacement are related by the angular frequency squared (i.e. ω^2), so knowing the frequency of the oscillator and the amplitude of the accelerometer output voltage, the displacement of the transducer is easily obtained.

Fig. 27 shows the response of a lead titanate-lead zirconate ceramic (PZT-5) disc in the "33" direction to an input drive of 150 volts. It is clear that the transducer response fluctuates considerably about the D.C. displacement level (which is shown dotted). The accelerometer used in this experiment was selected on the basis of its extended frequency response. Even so, the device was limited to a 10kc bandwidth.

*Gerson, Robert "Dependence of Mechanical Q and Young's Modulus of Ferroelectric Ceramics on Stress Amplitude," Jour. of Acoust. Soc. of Amer., Oct. 1960

In order to evaluate the "Q" of a transducer using this technique, it is necessary to have a transducer of sufficient size so that it will resonant in one of its modes within the 10kc frequency range of the accelerometer. Unfortunately, this implies dimensions on the order of three inches which proved larger than any of the ceramics available at the time of this experiment.

A second method for measuring small time varying displacements makes use of the fringe pattern appearing in a Michelson interferometer. In this technique one of the flat mirrors is mounted on a transducer and then driven by an A.C. voltage. After recombination the output beam is directed to a phototube. This tube is stopped down so that it sees only a small portion of the entire field, typically one fringe. As the driven mirror is displaced, the phototube alternately sees bright and dark fringes. If the output of the detector is monitored on an oscilloscope, the peak displacement of the driven mirror can be evaluated by noting the number of fringes which cross the detector per cycle of drive voltage. This approach to displacement measurement has the decided advantage that it is bandwidth limited only by response of the detector which will in all cases far exceed the operational frequencies of any focus spoiling modulator.

This technique was used in the laboratory and was found to yield results which were compatible with those of Fig. 27 in the lower frequency ranges. When the drive frequency was increased and approached the first radial resonant mode, the driven mirror was distorted and the entire fringe pattern was lost. This was not unexpected, but rather was predictable from a knowledge of radial mode shapes.

When the transducer was driven at the first thickness resonant frequency, high displacements were expected but not encountered. One explanation offered states that the high radial inertia forces present at the thickness resonance tend to clamp the periphery of the disc. Such a change in the boundary conditions may considerably lower the "Q". Nevertheless, this continues to be a problem area and remains a subject for possible future investigations.

SECTION XIII

CONCLUSION

This report has evaluated the modulation capabilities and power requirements of a Focus Spoiling type retrodirective modulator. In addition, equations and curves for a distributed mass transducer-mirror assembly have been developed and applied to the design of a typical modulator element. The power requirements for this unit have been evaluated as a function of bandwidth and presented in Fig. 20.

Experimentally, two solutions have been offered to the problem of measuring minute time varying displacements. The first, employing an accelerometer, offers extreme accuracy but relatively narrow frequency response. The second approach utilizes the fringe pattern in a Michelson interferometer and has reduced accuracy but virtually unlimited frequency response.

SELECTED BIBLIOGRAPHY

1. F. Jenkins and H. White, "Fundamentals of Optics", (McGraw Hill, New York, 1957).

2. W. Thomson, "Vibration Theory and Applications", (Prentice-Hall, Englewood Cliffs, New Jersey, 1965).

3. Endevco Corporation Publication, "Current Piezoelectric Technology", 1965.

4. D. Berlincourt and H. Jaffe, "Piezoelectric Transducer Materials", Proc. of IEEE, October 1965.

5. S. Timoshenko, "Vibration Problems in Engineering", (Van Nostrand, Princeton, New Jersey, 1955).

6. Lord Rayleigh, "Theory of Sound", (Dover, New York, 1945).

7. M. Born and E. Wolf, "Principles of Optics", (Pergamon, New York, 1959).

8. A. Conrady, "Applied Optics and Optical Design", (Dover, New York, 1957).

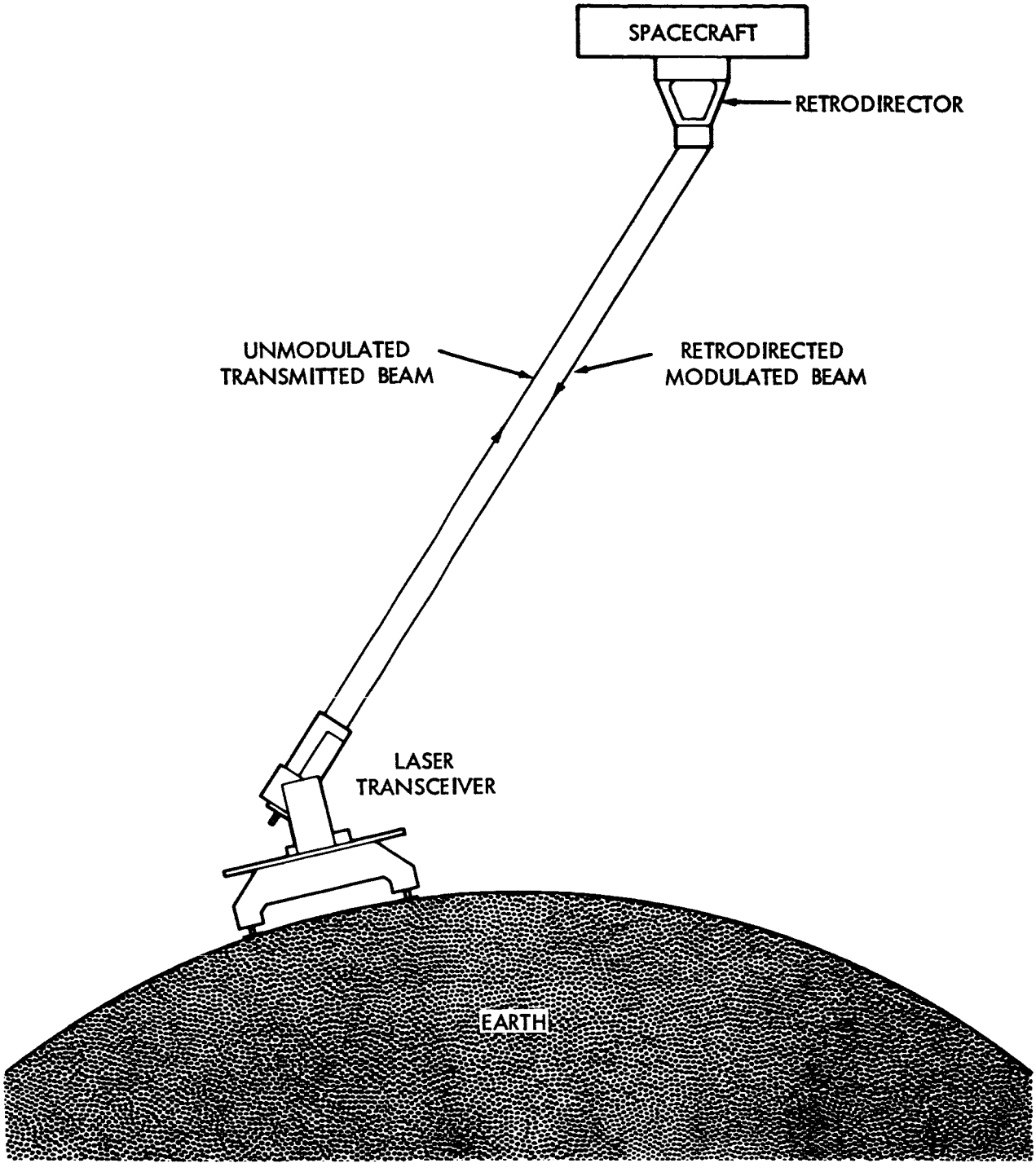

FIGURE 1 SATELLITE-TO-GROUND COMMUNICATIONS LINK

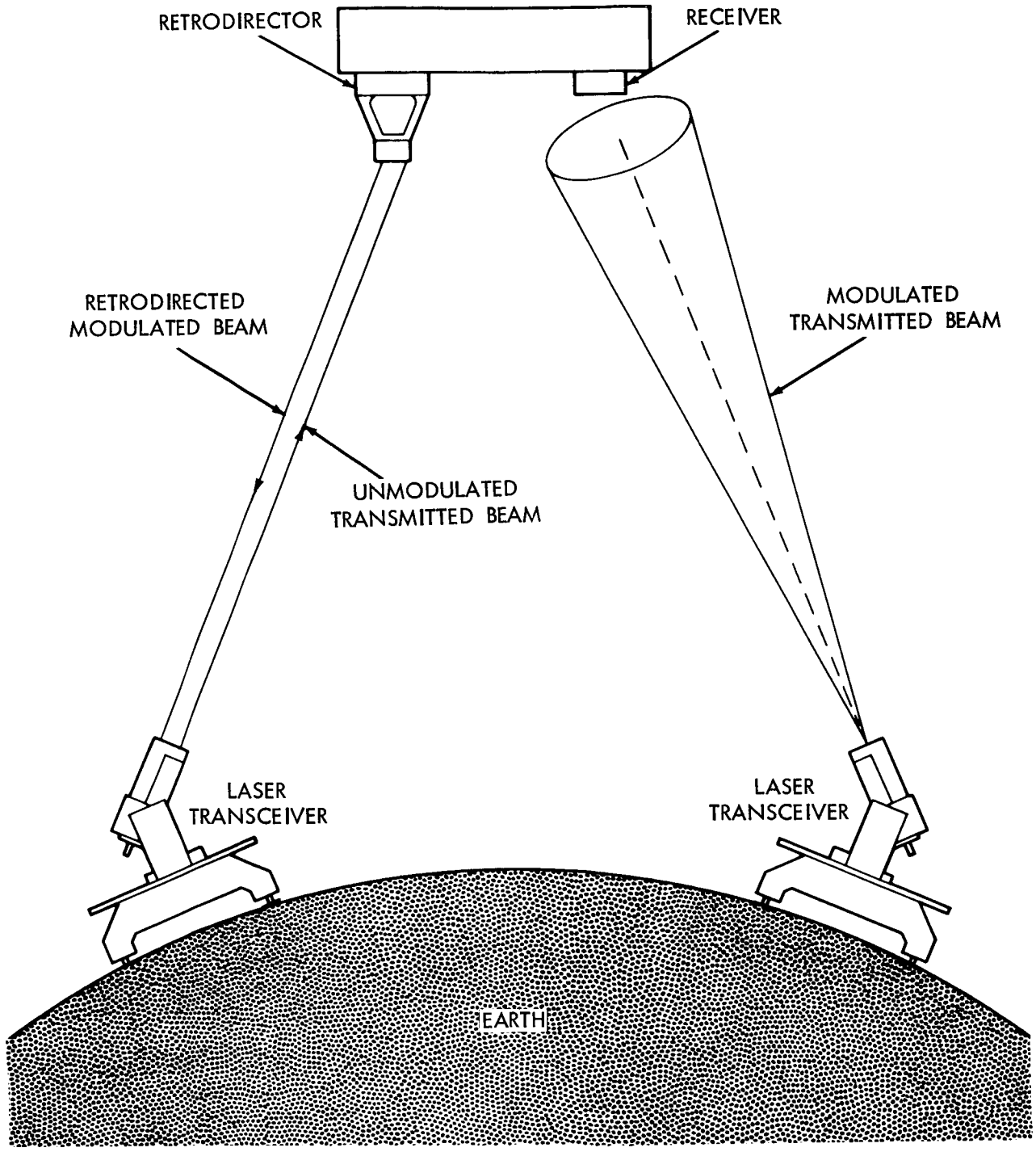

FIGURE 2 GROUND TO GROUND LASER COMMUNICATION LINK

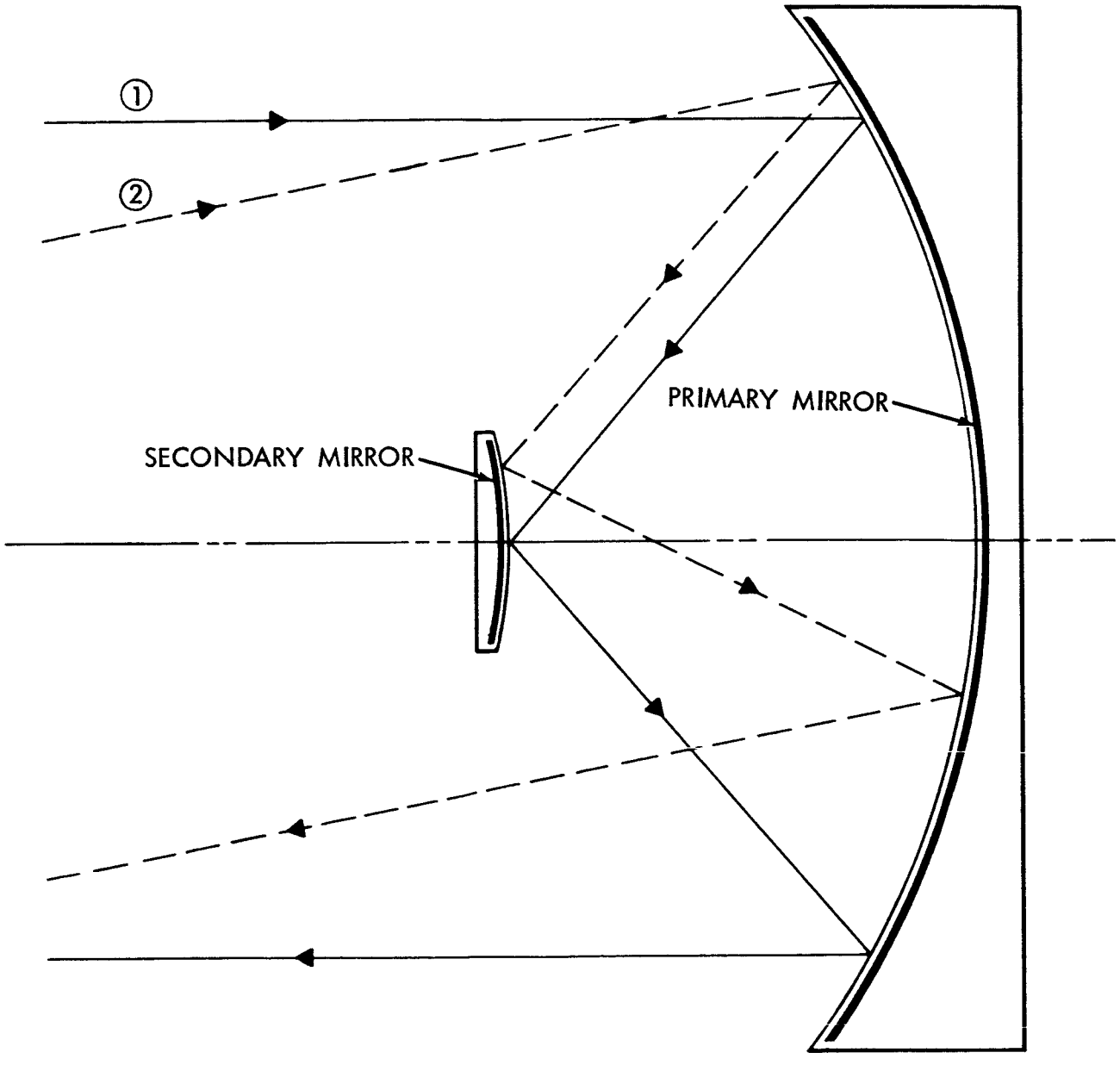

Fig. 3 CONCENTRIC RETRODIRECTOR

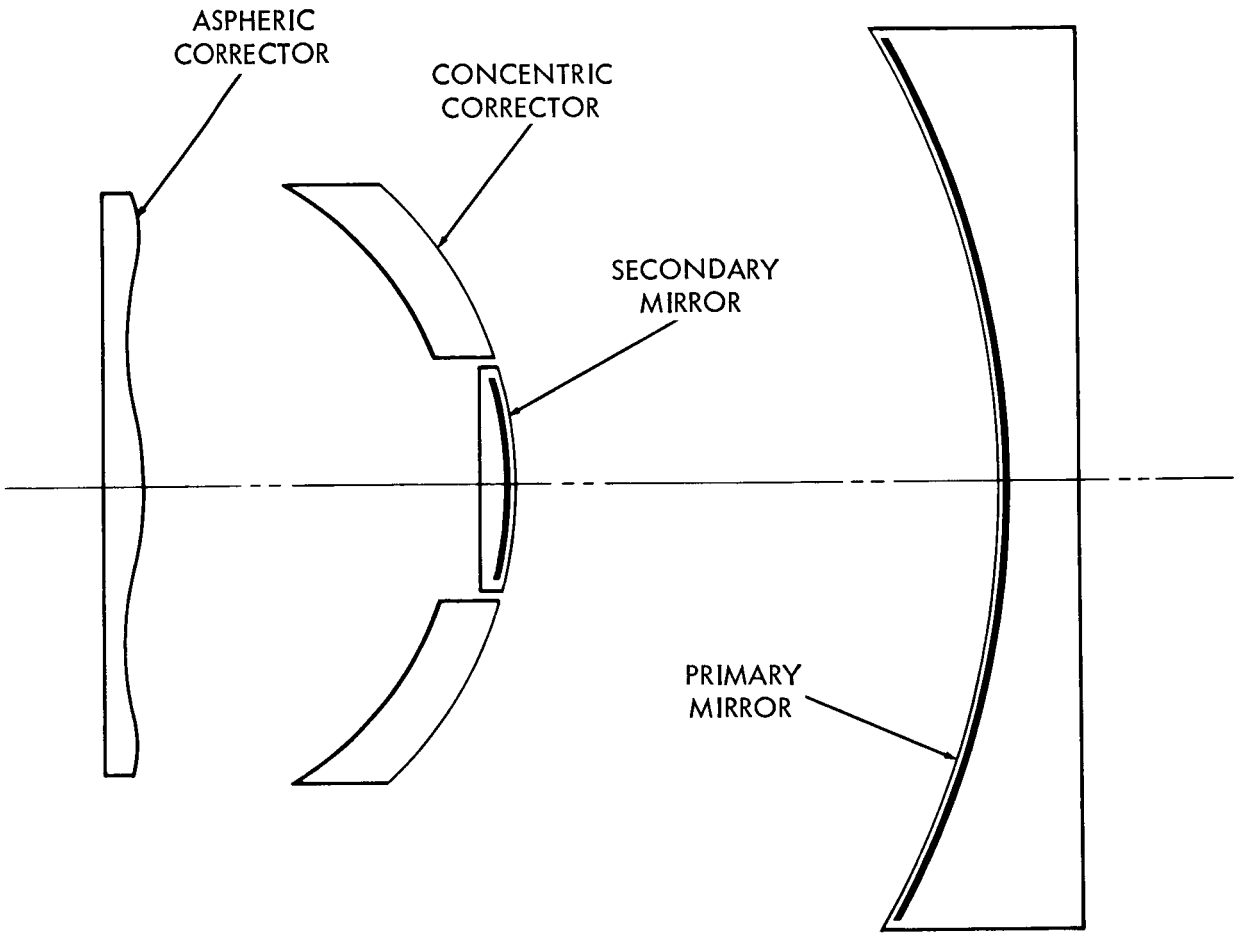

Fig. 4-- CORRECTED CONCENTRIC RETRODIRECTOR

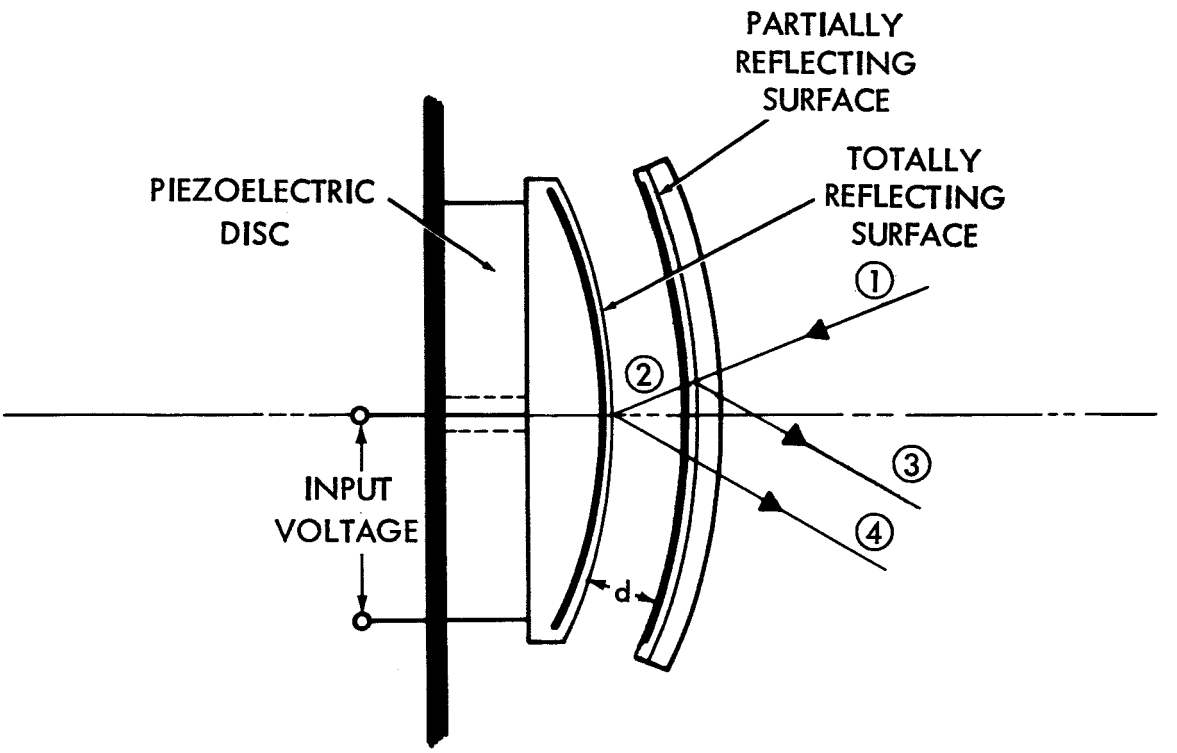

FIGURE 5 FABRY - PEROT INTERFEROMETER MODULATOR

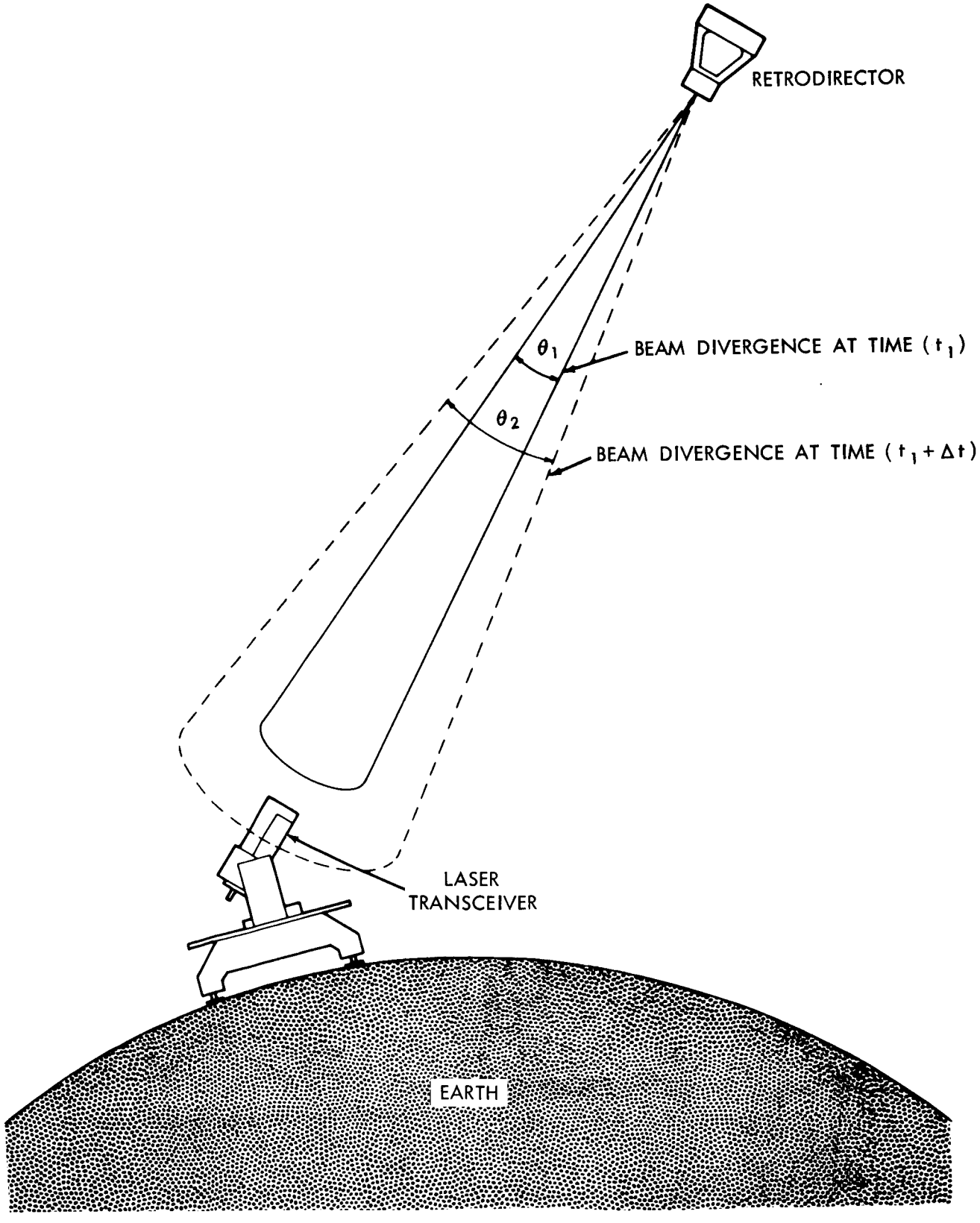

FIGURE 6 RETRODIRECTOR BEAM DIVERGENCE MODULATION

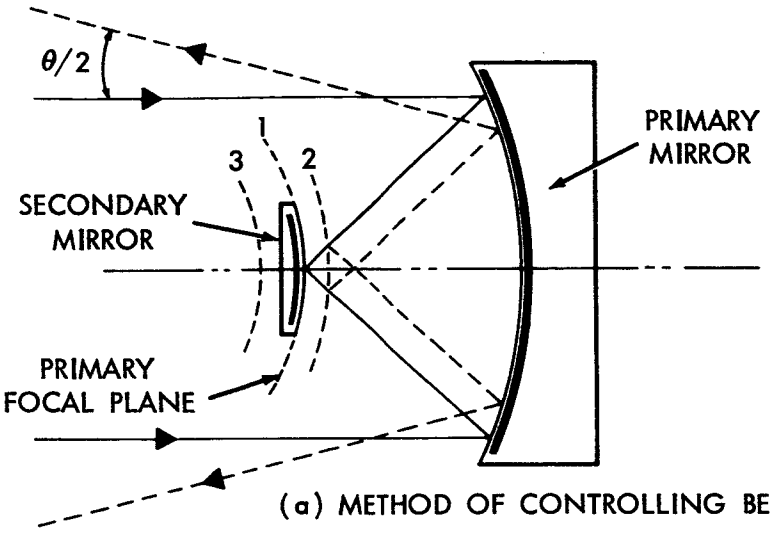

(a) METHOD OF CONTROLLING BEAM DIVERGENCE

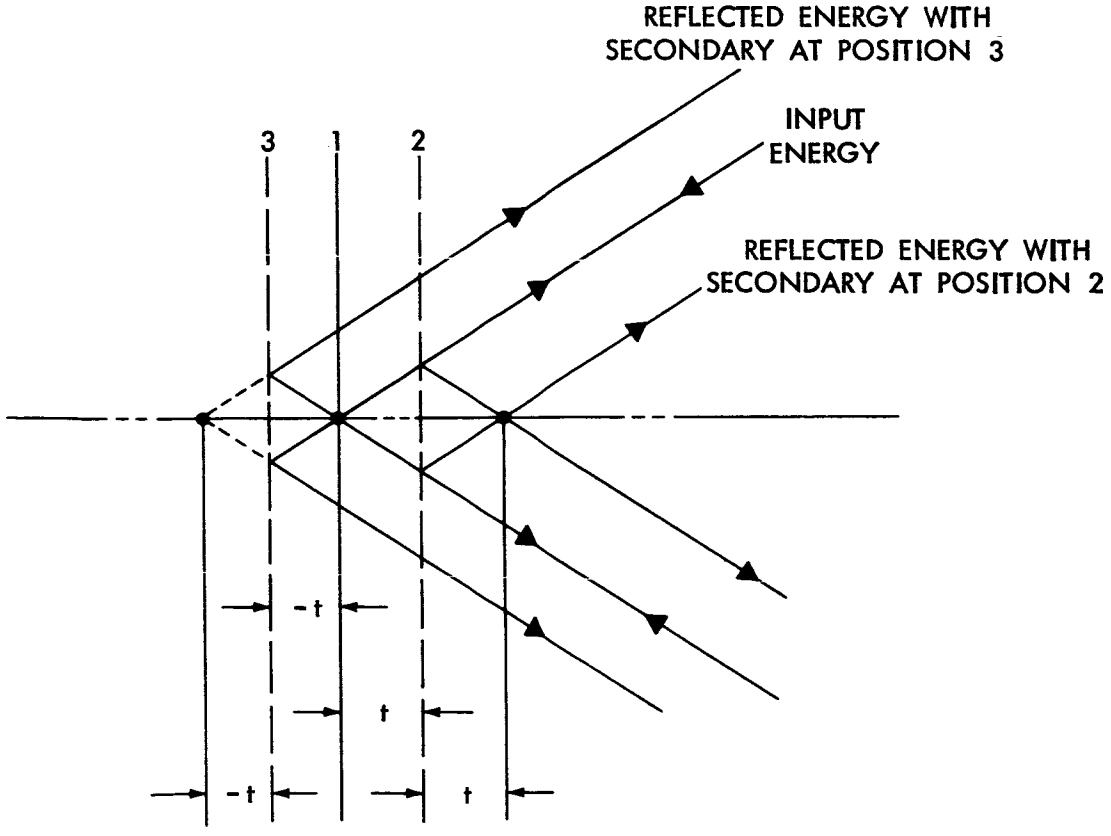

(b) PLANE MIRROR APPROXIMATION USED FOR DEVELOPING THE RELATIONSHIP BETWEEN θ AND t.

Fig. 7— RETRODIRECTOR FOCUS SPOILING

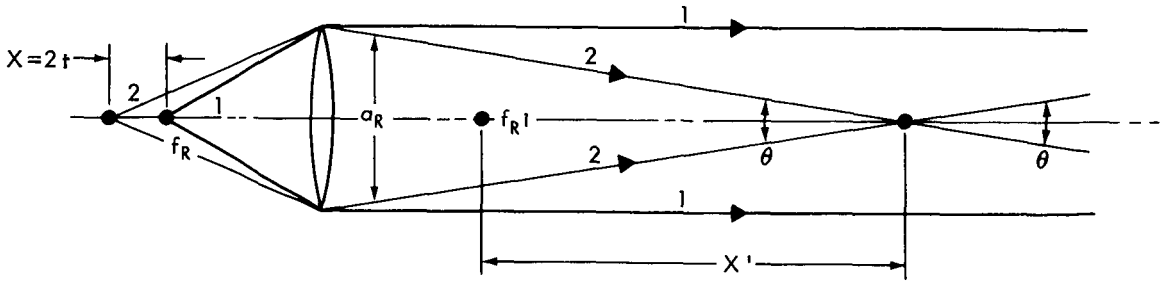

FIGURE 8 SCHEMATIC FOR DEVELOPING THE RELATIONSHIP BETWEEN RETURN BEAM DIVERGENCE AND SECONDARY DISPLACEMENT

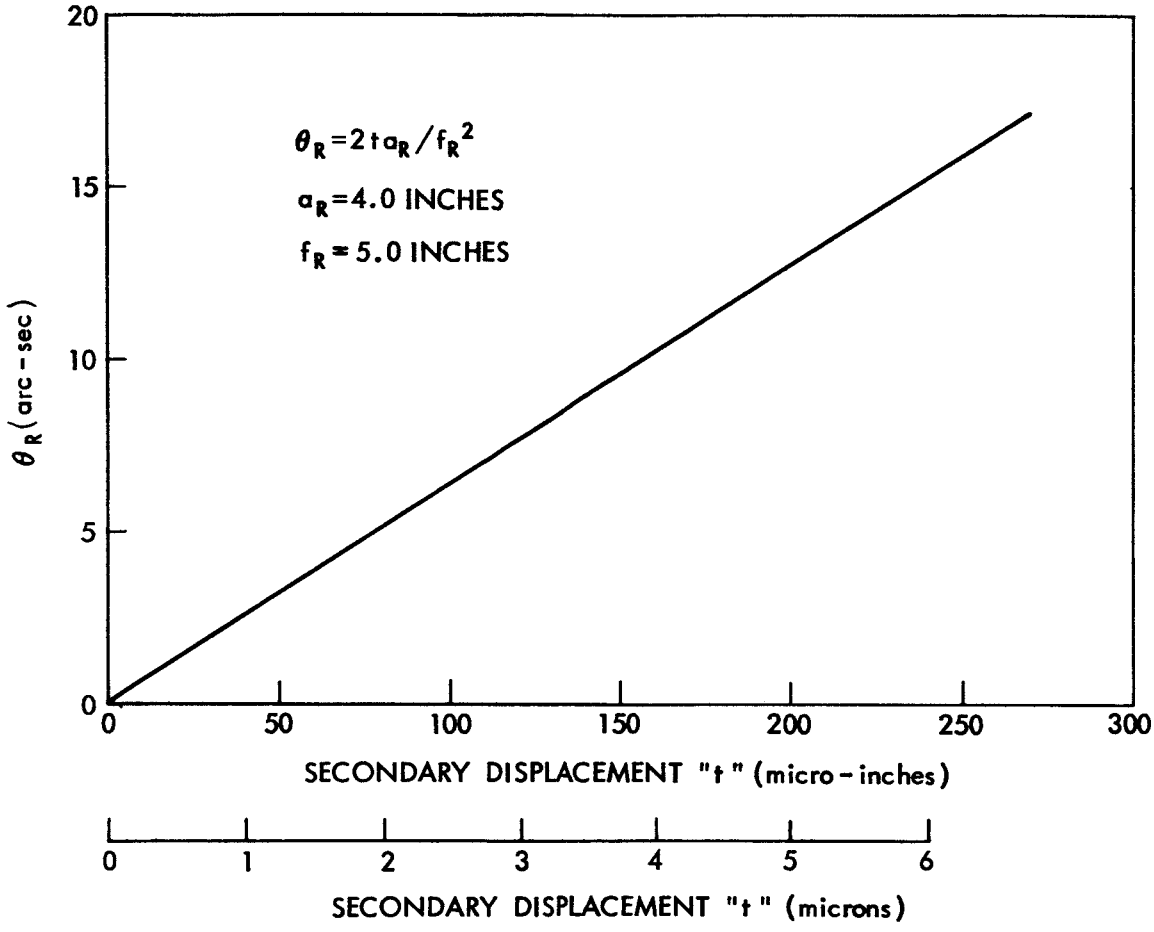

FIGURE 9 RETRODIRECTED BEAM DIVERGENCE (θ_R) VS. SECONDARY DISPLACEMENT (t)

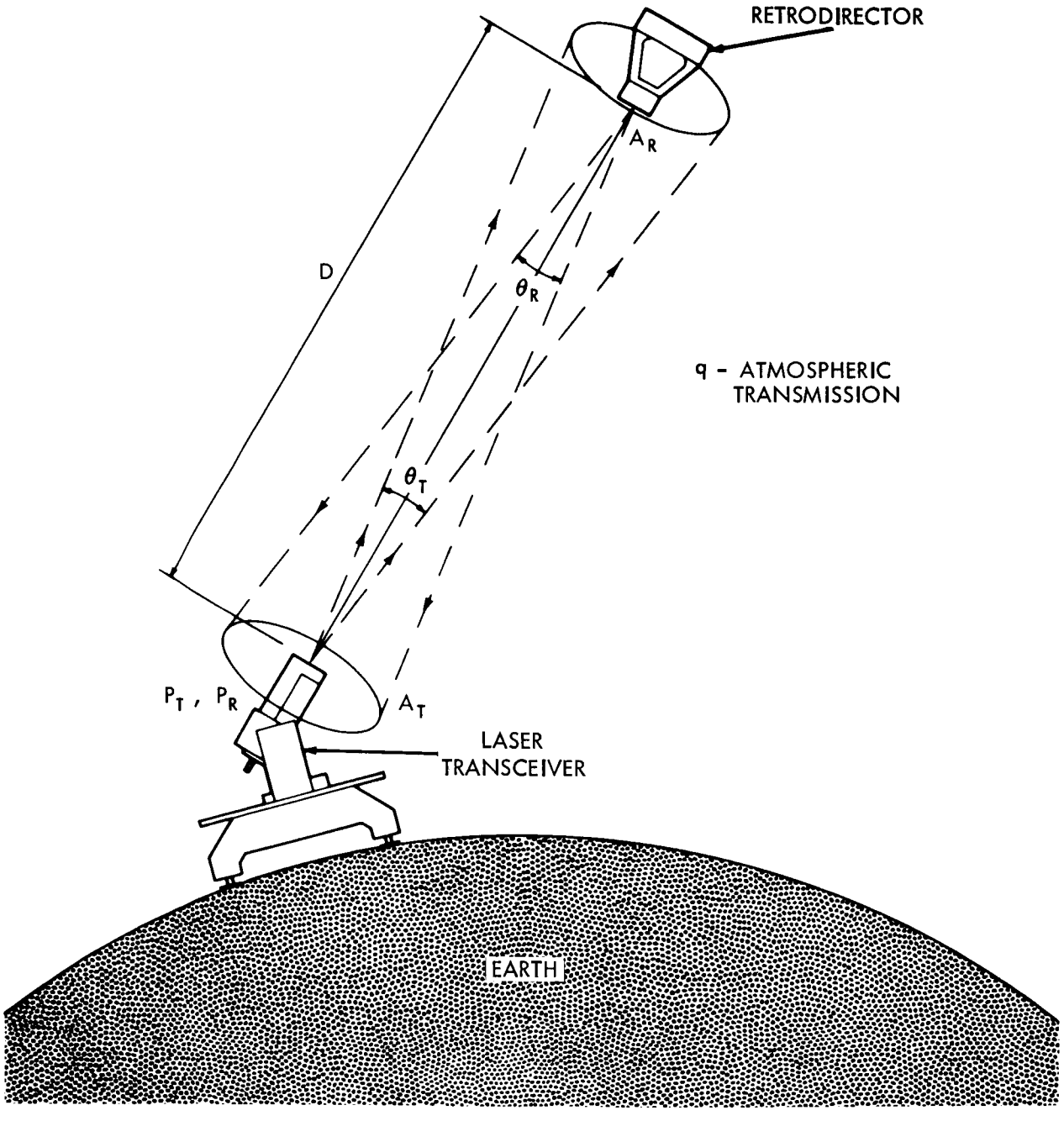

Fig. 10
IMPORTANT PARAMETERS FOR ENERGY CONSIDERATIONS

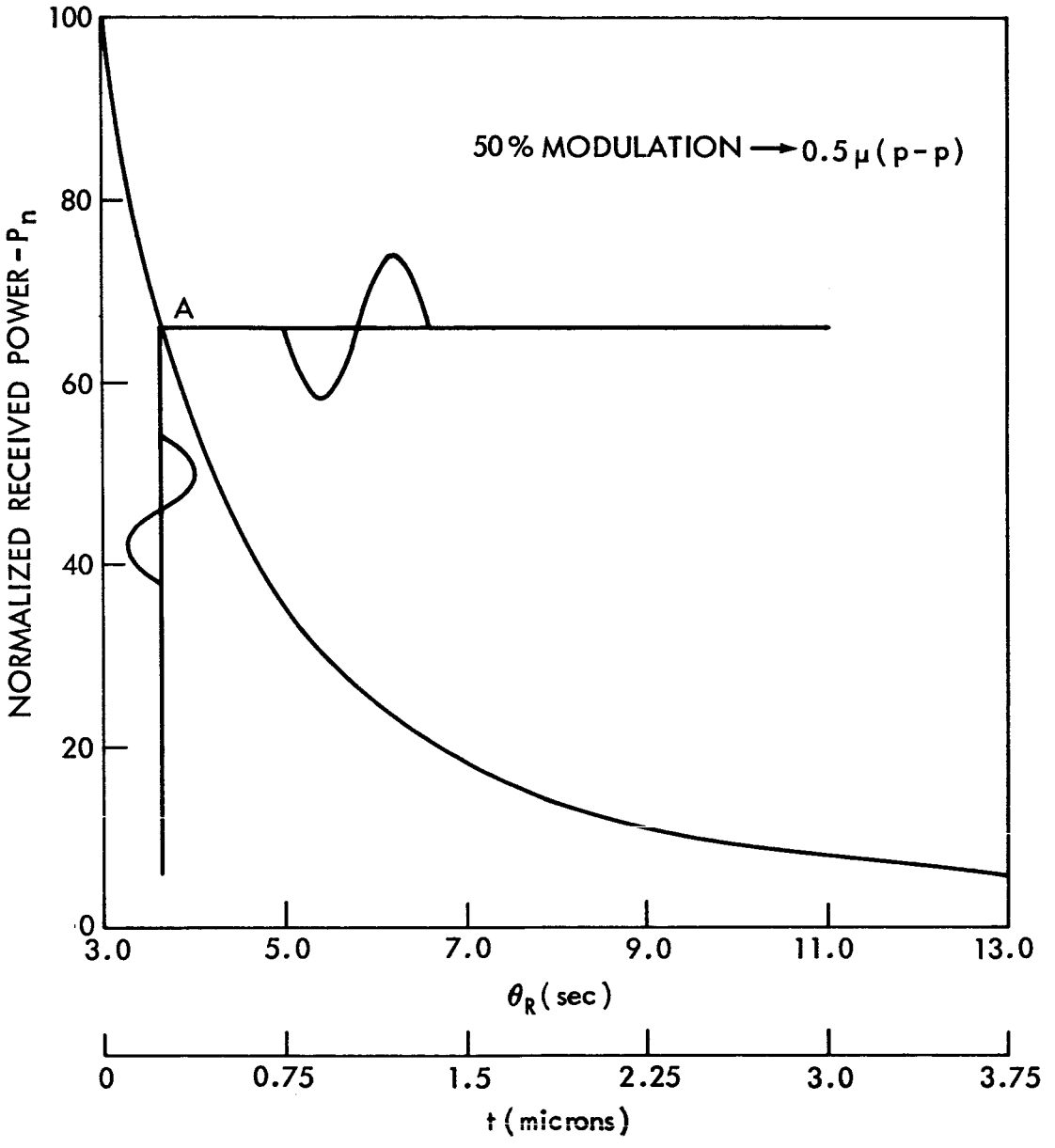

FIGURE 11 VARIATION OF RECEIVER SIGNAL STRENGTH WITH SECONDARY POSITION (t).

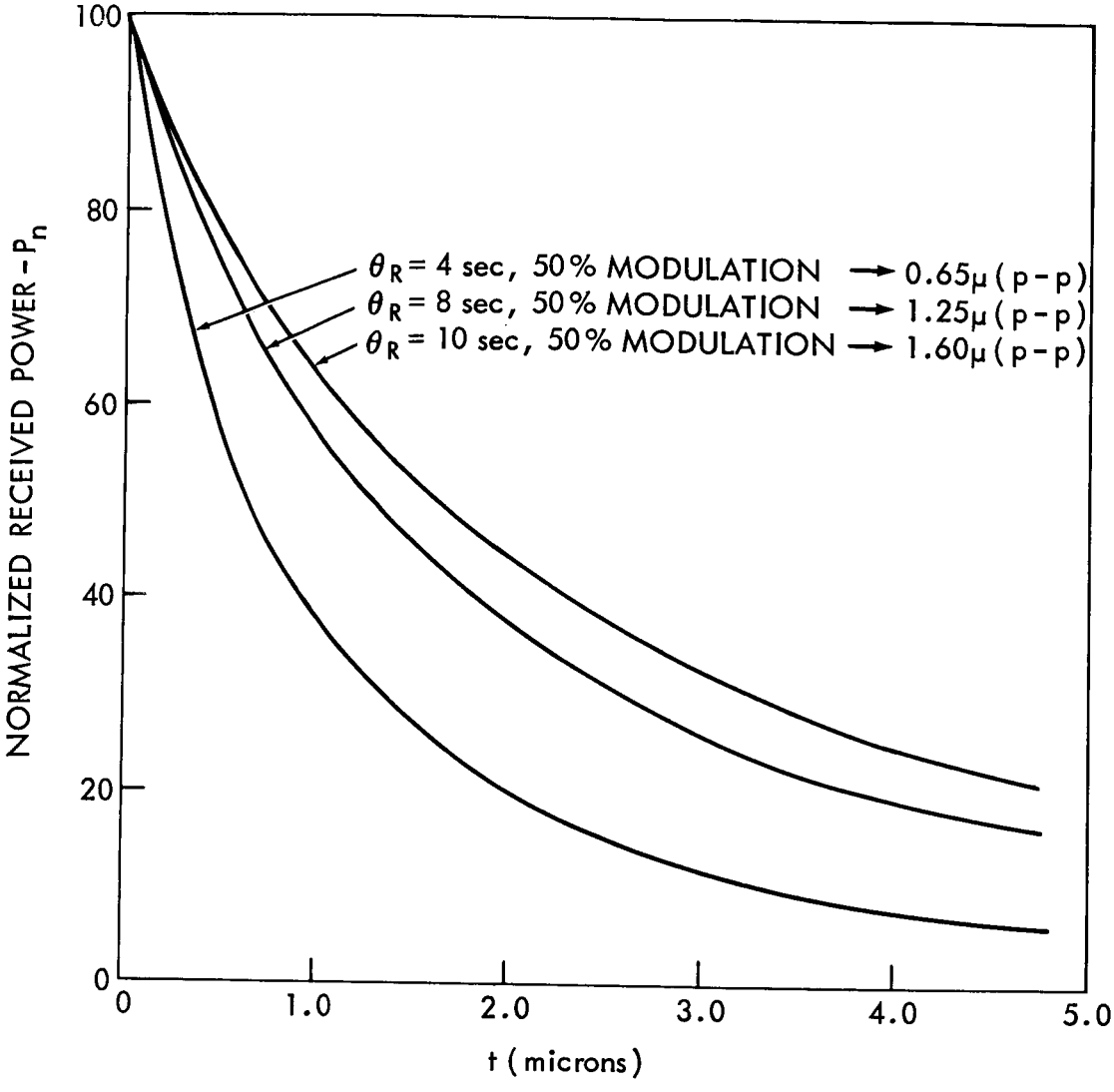

FIGURE 12 VARIATION OF RECEIVER SIGNAL STRENGTH WITH SECONDARY POSITION (t)

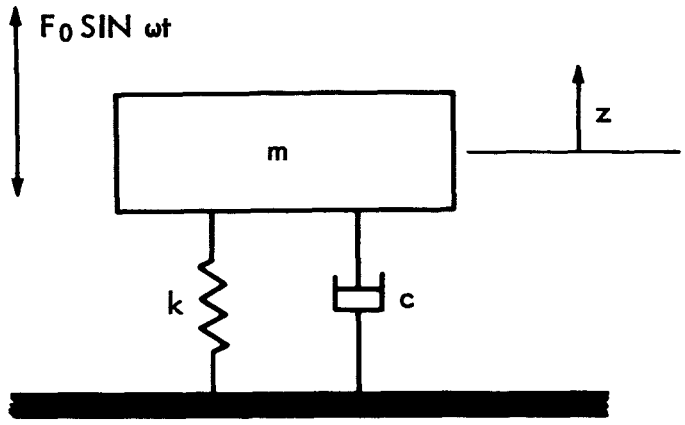

(a) LUMPED PARAMETER SYSTEM

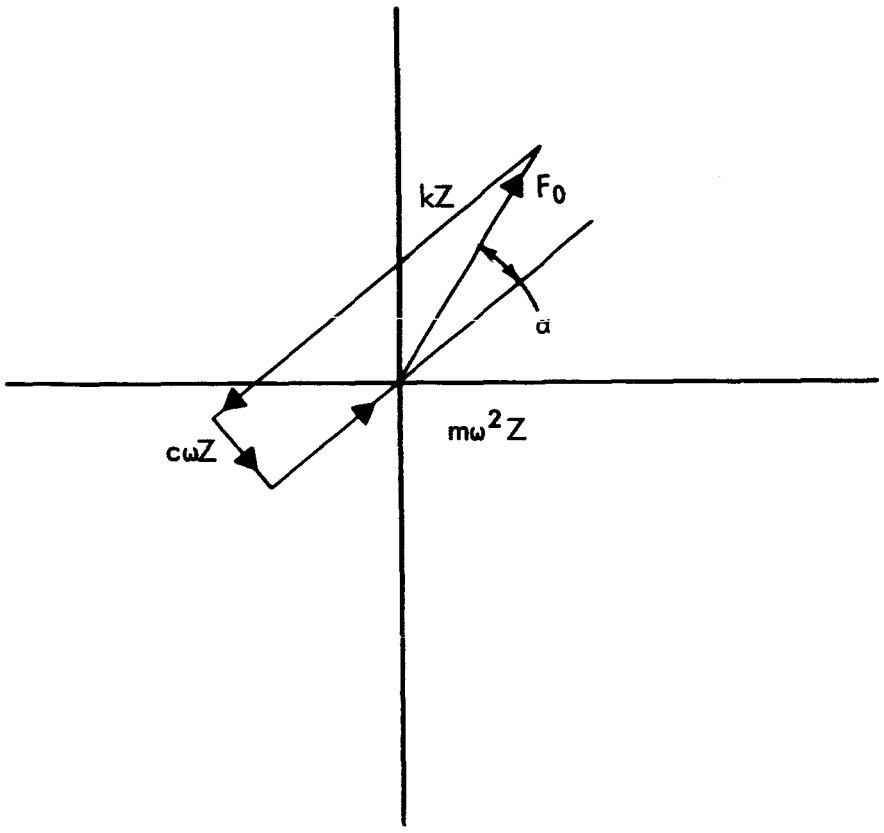

(b) PHASOR DIAGRAM OF THE FORCES ACTING

Figure 13 MODULATOR ELEMENT MODEL

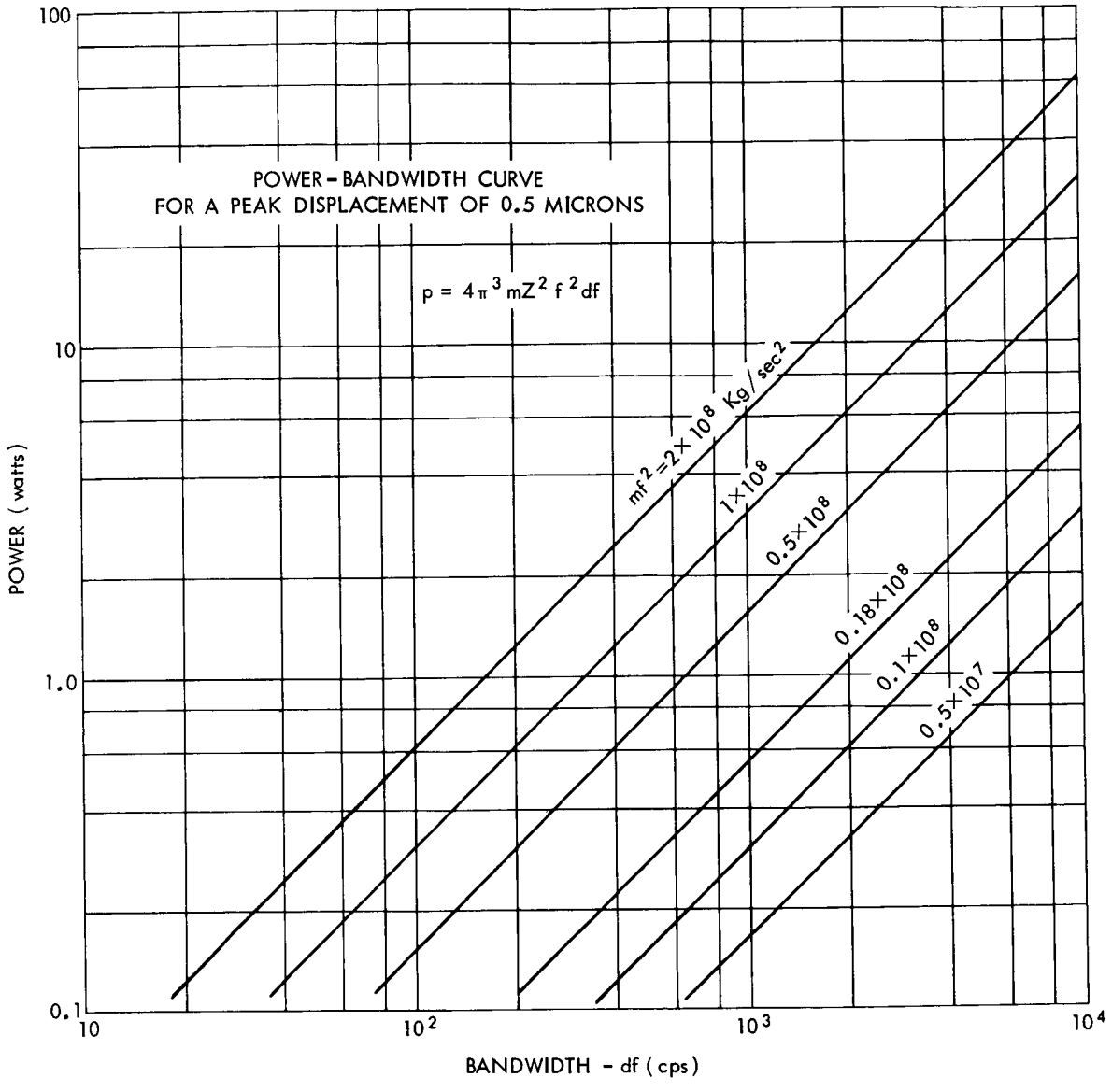
POWER - BANDWIDTH CURVE
FOR A PEAK DISPLACEMENT OF 0.5 MICRONS
$p = 4\pi^3 mZ^2 f^2 df$
$mf^2 = 2\times10^8$ Kg/sec^2
1×10^8
0.5×10^8
0.18×10^8
0.1×10^8
0.5×10^7
POWER (watts)
100
10
1.0
0.1
10
10^2
10^3
10^4
BANDWIDTH - df (cps)

FIG 14

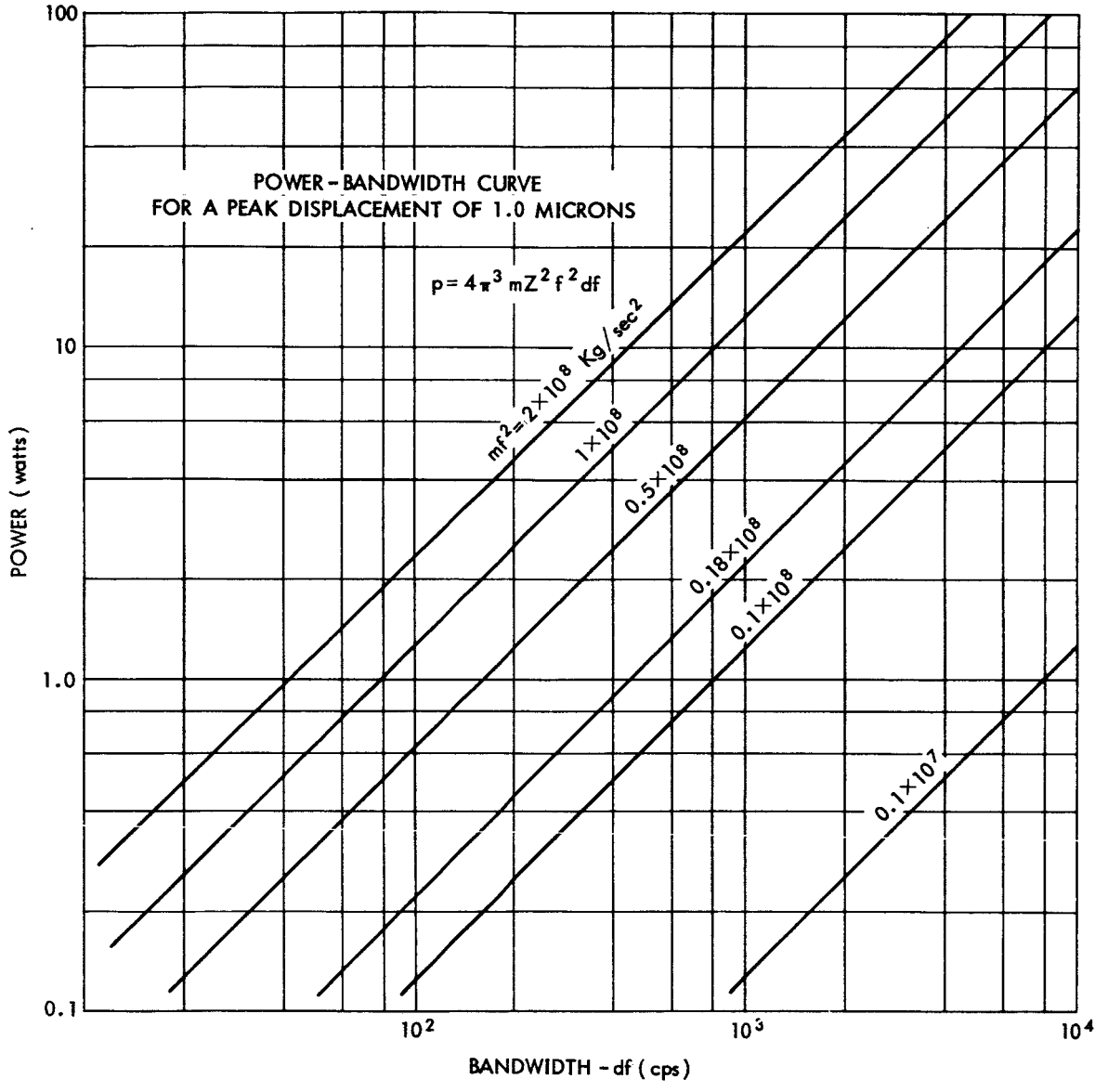
POWER - BANDWIDTH CURVE
FOR A PEAK DISPLACEMENT OF 1.0 MICRONS
$p = 4\pi^3 m Z^2 f^2 df$
$mf^2 = 2\times10^8$ Kg/sec^2
1×10^8
0.5×10^8
0.18×10^8
0.1×10^8
0.1×10^7
POWER (watts)
100
10
1.0
0.1
10^2
10^3
10^4
BANDWIDTH - df (cps)

FIG 15

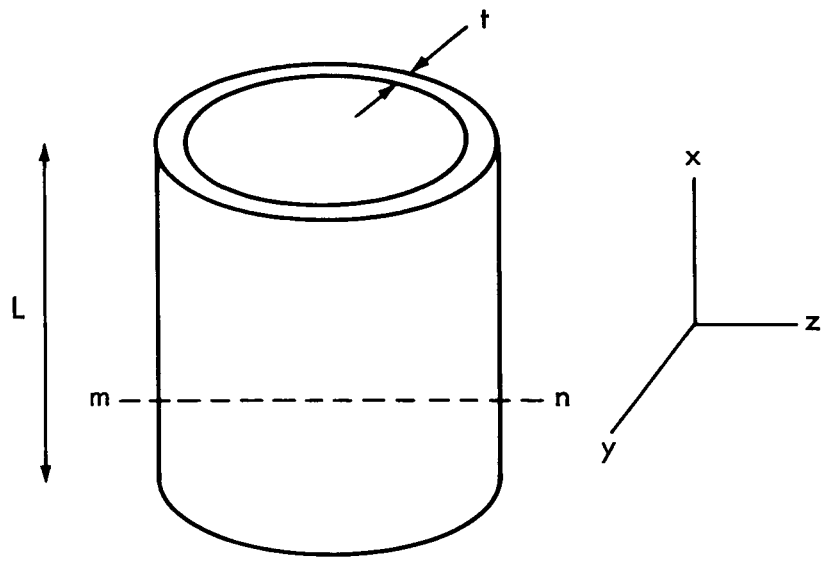

(a) TUBULAR TRANSDUCER

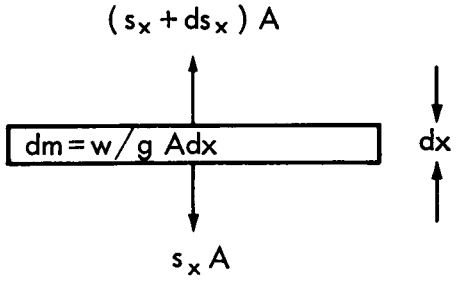

(b) FREE BODY DIAGRAM OF DIFFERENTIAL SECTION

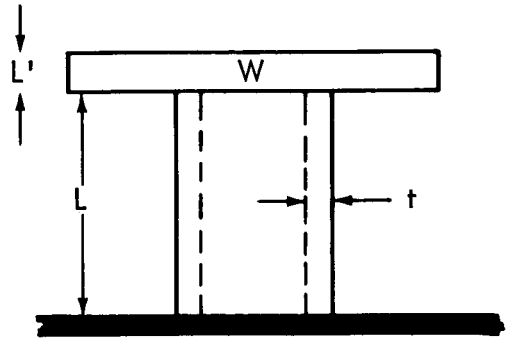

(c) TRANSDUCER WITH WEIGHT "W" ATTACHED TO FREE END

FIGURE 16 TRANSDUCER MODEL

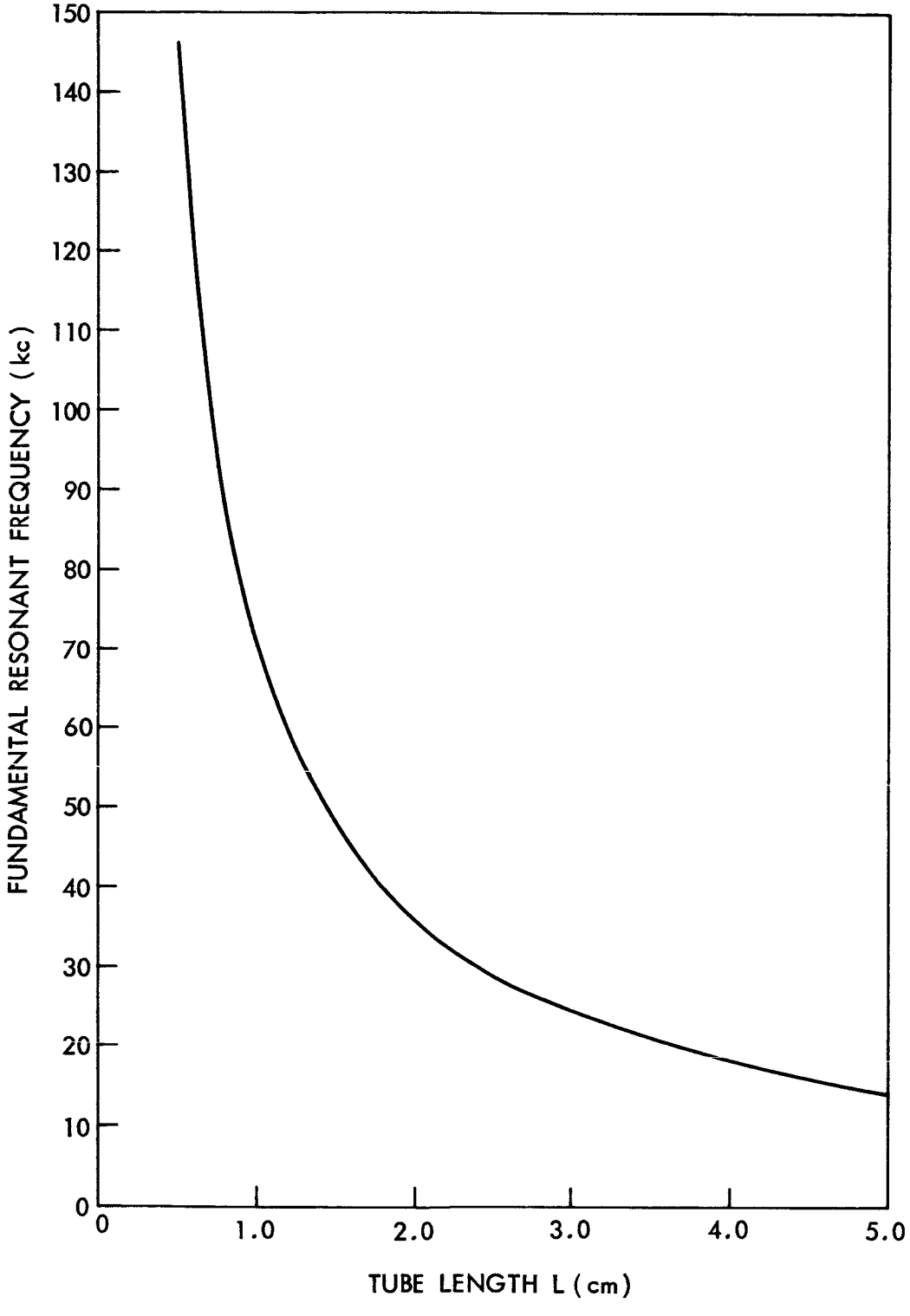

FIGURE 17 VARIATION OF FUNDAMENTAL RESONANCE WITH TUBE LENGTH

FIGURE 17

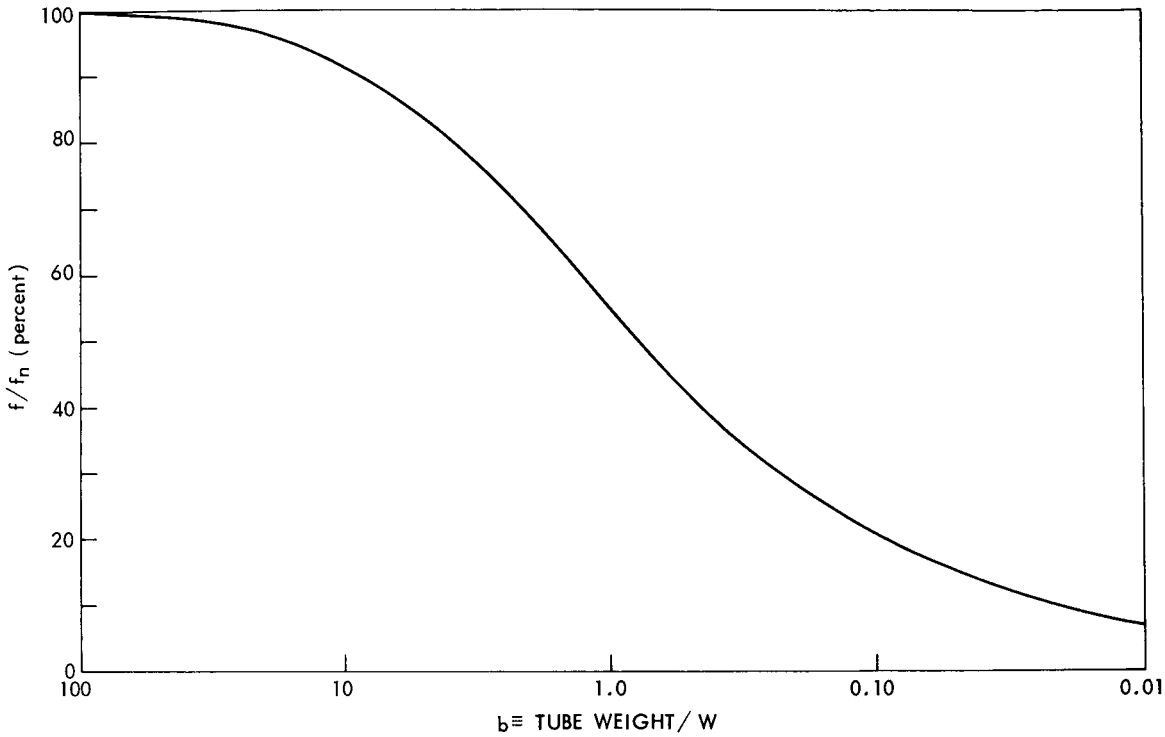

FIGURE 18 DEPENDENCE OF RESONANT FREQUENCY ON SECONDARY MIRROR WEIGHT "W"

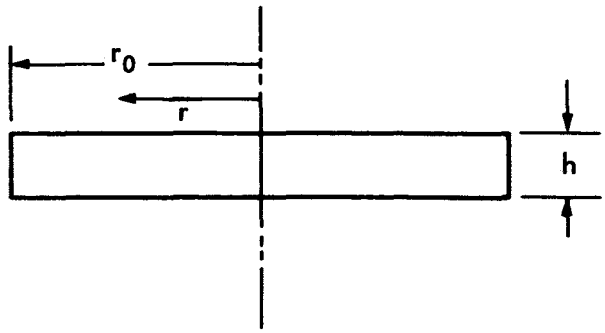

(a) CROSS-SECTION OF SECONDARY MIRROR

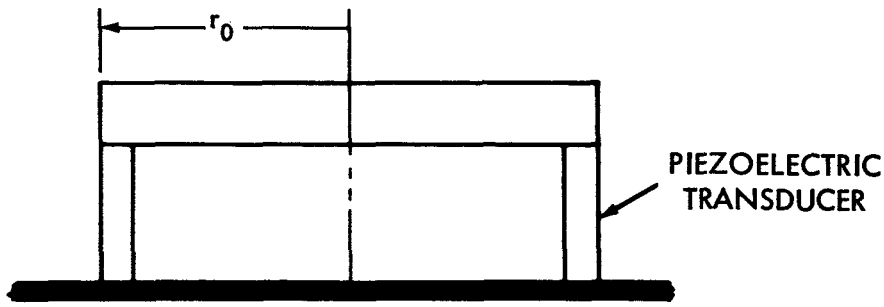

(b) SECONDARY SUPPORTED AT THE OUTER EDGE

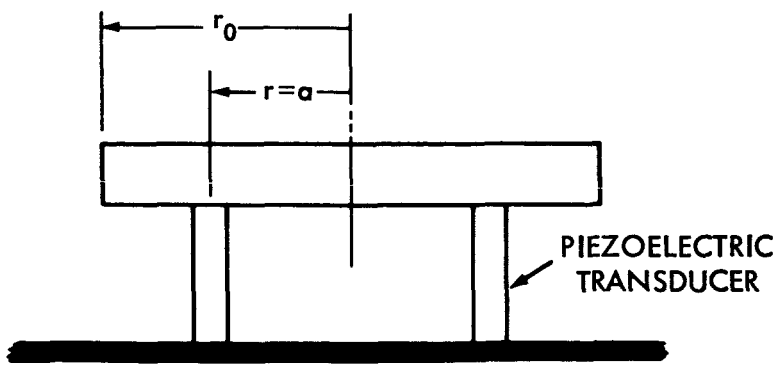

(c) SECONDARY SUPPORTED AT INTERIOR POINT "a"

FIGURE 19 SECONDARY MIRROR MOUNTING

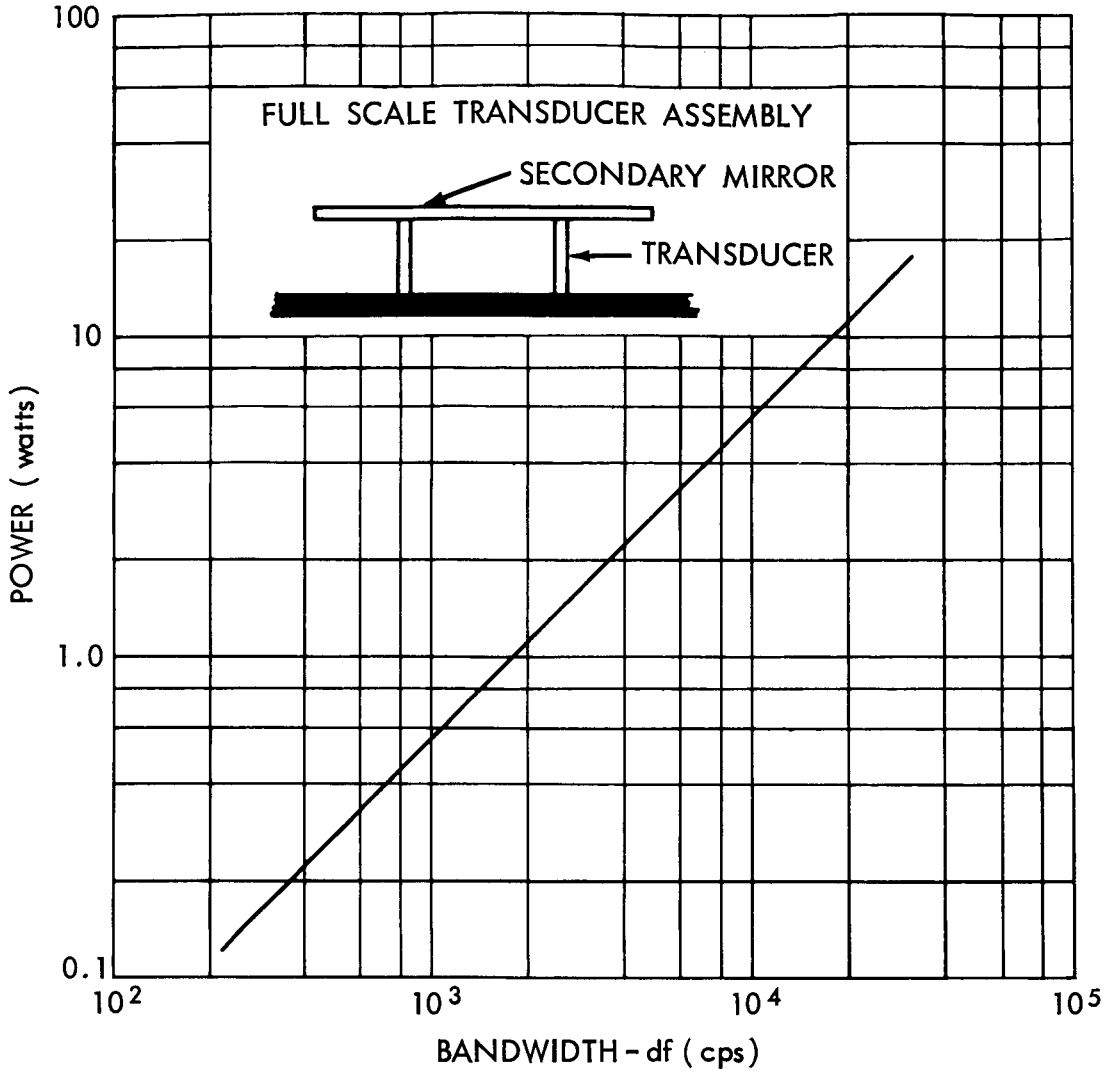

FIGURE 20 POWER - BANDWIDTH FOR DESIGNED TRANSDUCER

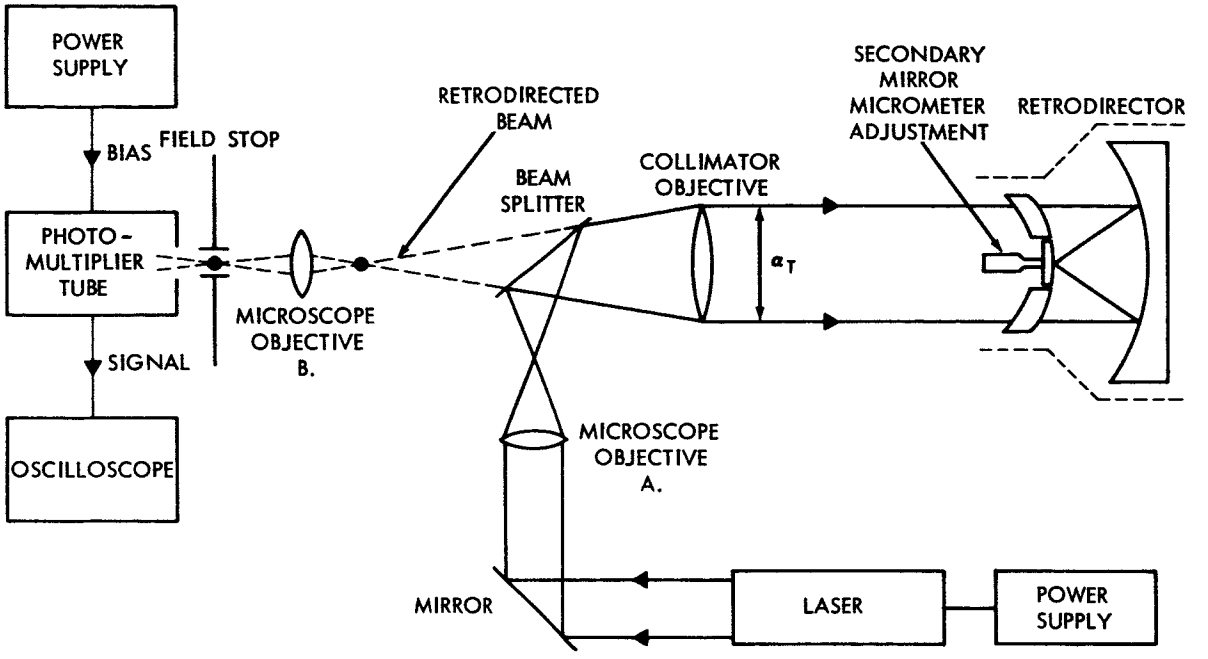

FIGURE 21 LABORATORY SCHEMATIC

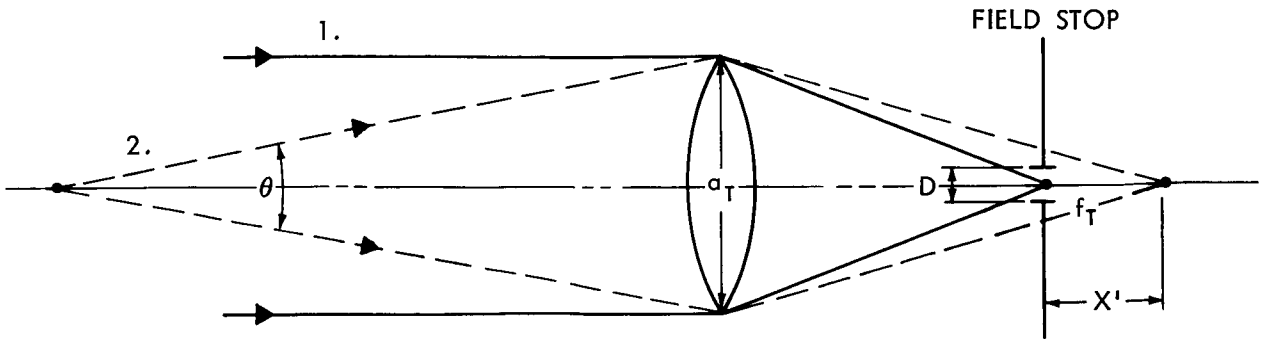

Figure 22 EQUIVALENT RECEIVER SYSTEM

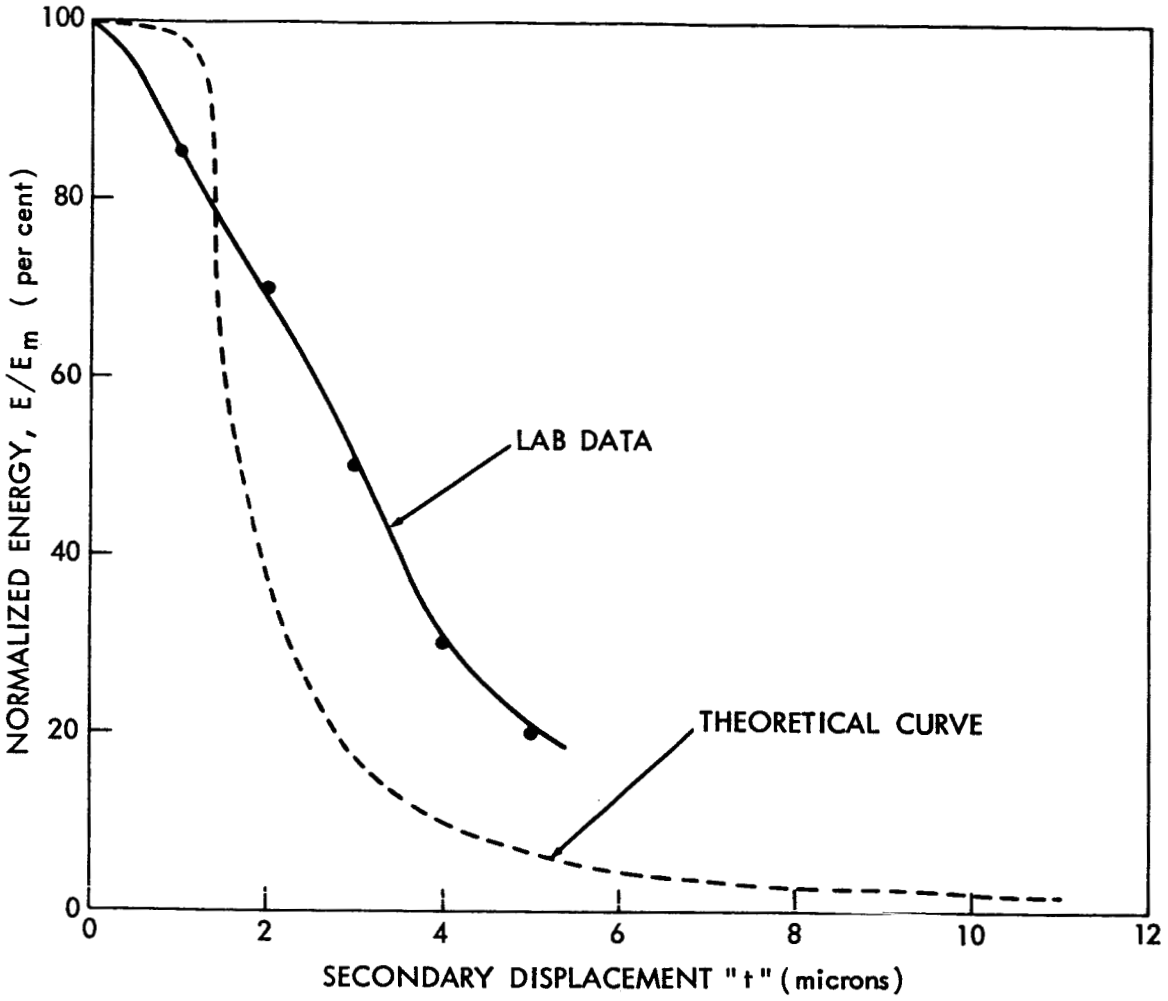

FIGURE 24. LABORATORY DATA

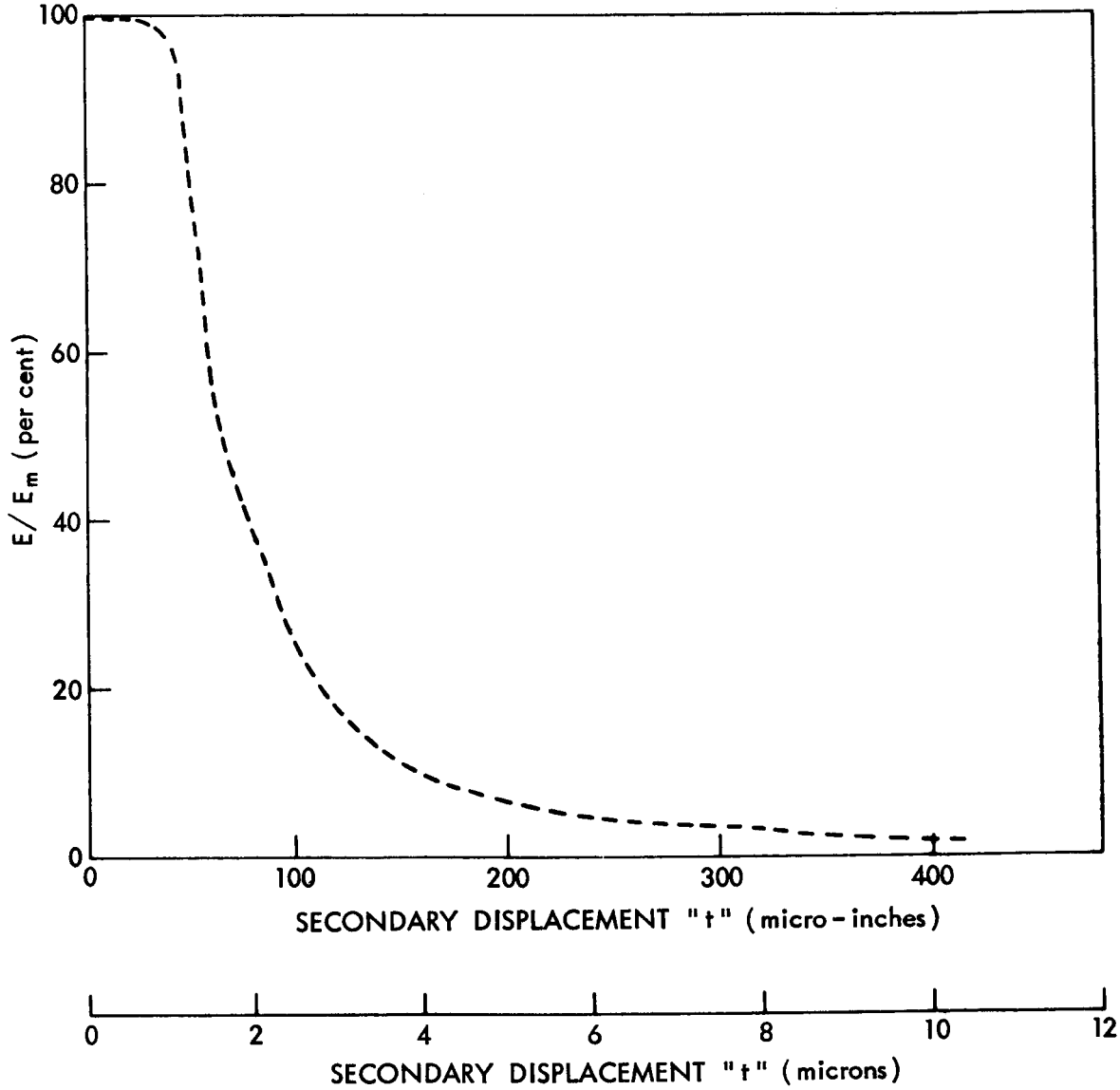

FIGURE 23. NORMALIZED PLOT OF RECEIVED ENERGY VS. SECONDARY DISPLACEMENT FROM PRIMARY FOCAL PLANE

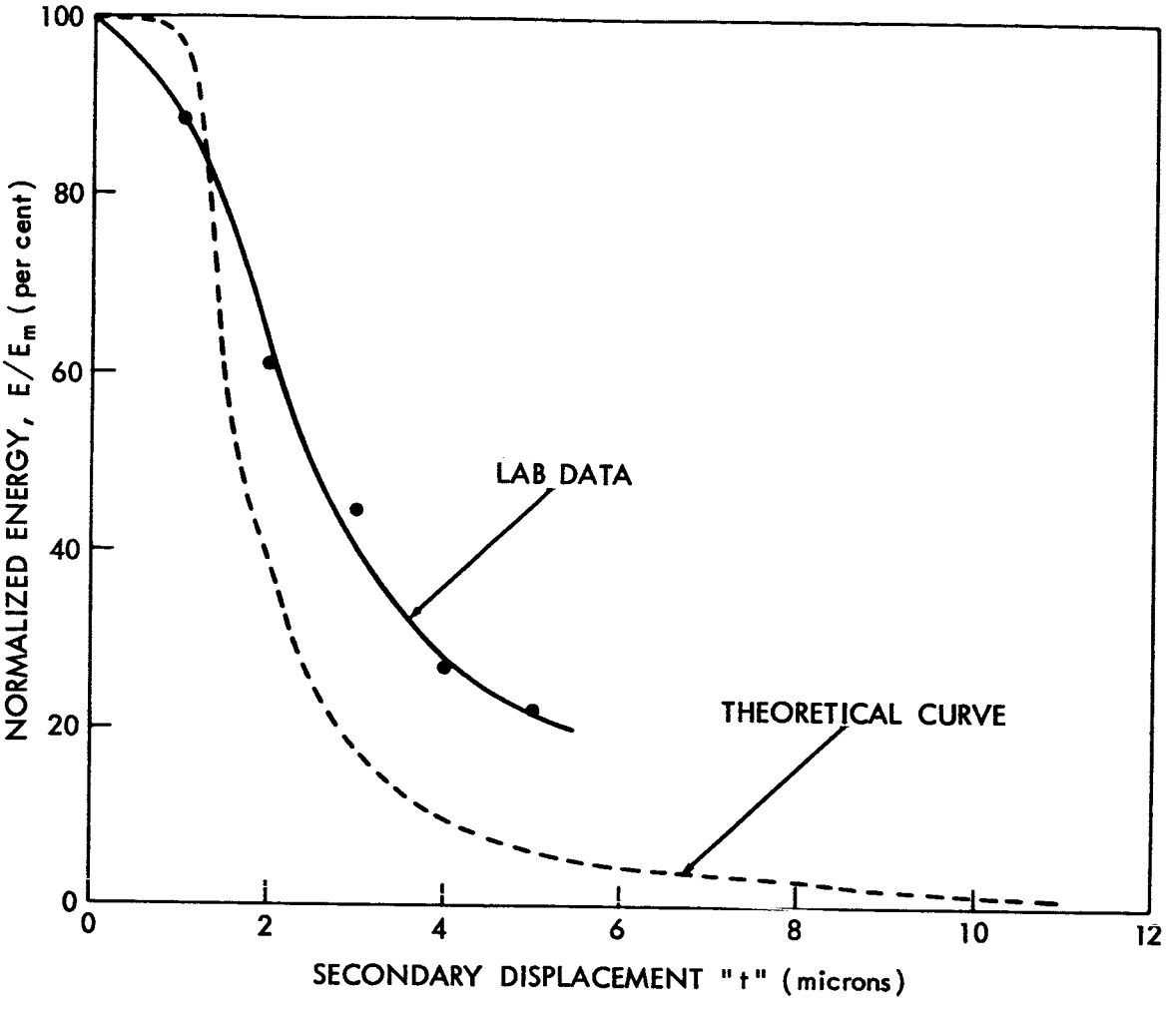

FIGURE 25. LABORATORY DATA

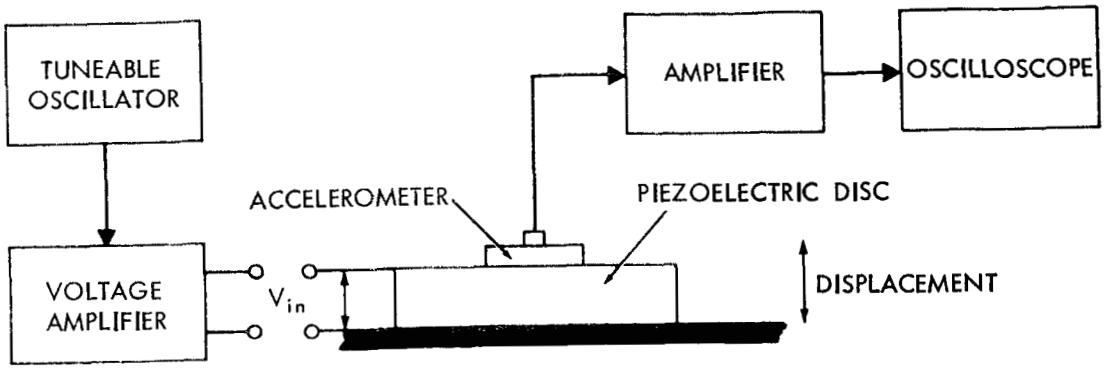

Fig. 26

ACCELEROMETER DISPLACEMENT MEASUREMENT SYSTEM

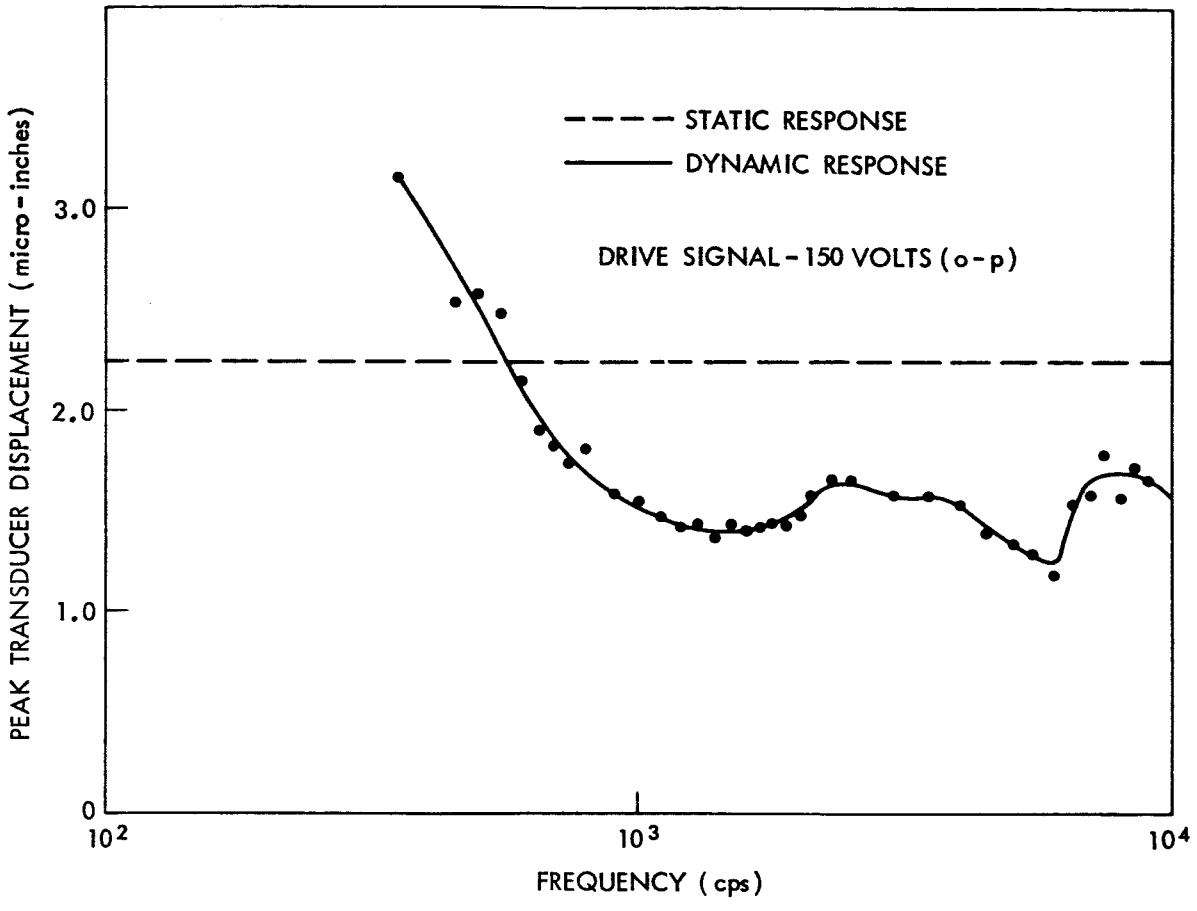

Fig. 27 DYNAMIC RESPONSE OF PIEZOELECTRIC DISC